UNIVERSIDADE DE LISBOA
FACULDADE DE CIÊNCIAS
DEPARTAMENTO DE BIOLOGIA ANIMAL

The relationship of ERG Potassium Channel with programmed cell death in the vertebrate developing limb

Rita Leiria Lopes Félix

Mestrado em Biologia Evolutiva e do Desenvolvimento

2010

UNIVERSIDADE DE LISBOA
FACULDADE DE CIÊNCIAS
DEPARTAMENTO DE BIOLOGIA ANIMAL

The relationship of ERG Potassium Channel with programmed cell death in the vertebrate developing limb

Rita Leiria Lopes Félix

Dissertação orientada por:
Professor Doutor Joaquín Rodríguez-León
Professora Doutora Gabriela Rodrigues

Mestrado em Biologia Evolutiva e do Desenvolvimento

2010

Acknowledgments

Muitas são as pessoas a que tornaram a realização desta tese possível (até ao último minuto!) e a quem tenho de agradecer.

Um muito obrigada ao Joaquín! Sem ele toda esta experiência não poderia ter acontecido. Obrigada por toda a disponibilidade e conhecimentos transmitidos, sempre com muito humor e boa disposição! Obrigada por tudo, foste um chefe impecável!

À Professora Gabriela que aceitou ser minha orientadora interna e sempre demonstrou interesse pelo meu trabalho, estando sempre disponível para qualquer dúvida ou problema.

Ao Instituto Gulbenkian de Ciência, uma instituição com excelentes condições e espírito científico.

À Catarina, pelo *erg* e todo o apoio nesta jornada! À Raquel, sempre incansável e paciente a ensinar e a aturar maluqueiras, mesmo fora de horas…

À Rita, que merece mais que duas páginas de agradecimentos por toda a ajuda ao longo do trabalho! À Joana e as suas manias, à Teresa, à Diana e ao Nando por toda a companhia!

Ao grupo do Moisés, que também sinto ser um pouco meu, em particular à Isabel, Sofia e Arnon, com quem a vida no laboratório não teria sido tão divertida.

Aos amigos e à família, em especial à mãe pelo apoio incondicional e "mãetrocínio" ao longo de todo este percurso!

Obrigada a todos!

Abstract

A proper rate of programmed cell death (apoptosis) is vital to maintain normal tissue homeostasis, limit organ growth, eliminate unnecessary cells and undergo normal development. During limb development the apoptotic areas are controlled by a tight interaction between different genes that are responsible for the specific localization of this domains in the limb bud. In here we show that ERG, an outward potassium channel belonging to the *ether-a-go-go* family of voltage-gated potassium channels, is expressed, in proper time and space, in the apoptotic areas. We have studied the relevance of *erg* during the apoptotic process during the formation of digits in species with a different pattern of interdigital cell death, namely duck and chicken. We have performed loss-of-function experiments through *in ovo* electroporation of a construct with specific RNAi against *erg* and by implantation of beads soaked in an ERG inhibitor. The phenotypes obtained show a decrease in apoptosis in the interdigital space. Moreover, inhibition of *erg* action is followed by downregulation of different molecules involved in the apoptotic process. We have also unraveled the relationship of *erg* with different signaling pathways known to be involved in the triggering of cell death during limb development like FGFs, BMPs and Retinoic Acid. Most importantly, our findings show that *erg* is a key player in the establishment of interdigital cell death during digit development. Our results support a model in which *erg* is responsible for detachment

Keywords: ERG Potassium channel, apoptosis, digit development, FGF and BMP signaling

Resumo

Uma taxa de morte celular programada (apoptose) adequada é vital para a manutenção da homeostase dos tecidos, limitação do crescimento celular, eliminação de células indesejadas e para o decorrer normal do desenvolvimento no organismo. O desenvolvimento do membro é uma situação paradigmática em que a morte celular programada tem um papel central na morfogénese (Saunders, 1966). Desta forma, o membro de vertebrados é um dos melhores modelos para estudar o mecanismo apoptótico.

Durante o desenvolvimento dos vertebrados, os primórdios das extremidades apresentam áreas específicas de morte celular programada. As zonas necróticas anterior e posterior (ANZ e PNZ) são responsáveis por definir a forma mais proximal da extremidade do membro - o estilopódio e o zeugopódio. Já o *opaque-patch*, na parte central do mesênquima, vai definir os elementos esqueléticos do zeugopódio, o rádio e a ulna. Por último, as áreas necróticas interdigitais (INZs) vão esculpir a forma final dos dedos (Zuzarte and Hurlé, 2005). O controlo e localização específica destas áreas de morte celular programada é feito através de uma delicada interacção entre diferentes genes durante o desenvolvimento do membro.

Das moléculas sinalizadoras que controlam a indução da apoptose, destacam-se as da família dos BMPs e FGFs (Ganan et al., 1996, Montero et al., 2001). De facto, para que a indução da morte celular programada seja eficaz, estas duas vias de sinalização devem actuar em conjunto (Montero et al., 2001). A actividade conjunta de BMPs e FGFs resulta na activação da expressão de genes específicos que são responsáveis, inicialmente, pela perda de comunicação celular no mesênquima, o que constitui um processo crucial para que a apoptose tenha lugar (Hurle and Fernandez-Teran, 1983; Martin-Bermudo et al., 1998). No final, a cascata das caspases é activada, o que culmina com a destruição controlada da célula (Zuzarte-Luis et al., 2004).

A morte celular programada partilha muitos mecanismos com outros processos celulares como a proliferação e diferenciação. No entanto, a resposta à mesma proteína pode resultar em diferentes efeitos, dependo do contexto celular. No mesênquima da extremidade do membro observa-se que os BMPs podem induzir tanto diferenciação condrogénica como morte celular. De forma semelhante, os FGFs são, inicialmente, responsáveis pela sobrevivência da célula enquanto que, mais tarde, induzem a sua apoptose (Ganan et al., 1996; Montero et al., 2001). Para além das numerosas cascatas genéticas que se sabem estar envolvidas na indução e desenvolvimento do membro de vertebrados existem também mecanismos epigenéticos que influenciam a padronização do mesmo. Desta forma, fecha-se o ciclo entre informação genética e o ambiente celular. Entre estes mecanismos epigenéticos destacam-se os fluxos iónicos (Altizer et al., 2001). Estes têm sido implicados em diferentes processos tais como a migração, morte e diferenciação celulares (Morokuma et al., 2008). Foram também observados durante o desenvolvimento embrionário, onde são responsáveis, por exemplo, pela correcta formação das extremidades (Altizer et al., 2001).

A acção de moléculas sinalizadoras na indução da apoptose tem sido principalmente estudada nas INZs. Resumidamente, a actividade do Ácido Retinóico activa a expressão de BMPs no espaço interdigital o que, em conjunto com a expressão de FGFs já existente nessa zona, induz a apoptose no interdígito (Rodriguez-Leon et al., 1999; Montero et al., 2001). No entanto, esta indução de morte celular programada deve ser precedida pela inibição da expressão de FGF8 na ectoderme distal do interdígito (Hernandez-Martinez et al., 2009). No final, a confluência de vários mecanismos nessas zonas resulta numa morte celular em massa nas áreas do interdígito.

Este trabalho procura mostrar a existência de um elo de ligação entre a actividade de ERG, um canal de saída de potássio, e a morte celular programada durante o desenvolvimento dos membros. ERG pertence à família ether-a-go-go de canais de potássio dependentes de voltagem, e é detectado nas áreas apoptóticas do autopódio de galinha (*Gallus gallus*) e pato (*Anas platyrhynchos*). O facto de estar presente em todo o espaço interdigital de espécies com dedos livres (galinha) e só na parte mais distal do interdígito em pato onde a morte fisiológica ocorre, sugere que a sua função pode estar conservada evolutivamente. O padrão de expressão deste canal de potássio é detectado nas INZs, de forma espacial e temporalmente conservada nos dois organismos.

Para analisar a função de ERG, realizaram-se estudos de perda de função através da electroporação *in ovo* de uma construção de RNAi específico para o gene em estudo. Outra abordagem usada para o mesmo fim foi a implantação de microesferas embebidas num inibidor químico do canal, de forma a possível bloquear funcionalmente a dinâmica de potássio intracelular no membro em desenvolvimento. A perda de função de ERG conduz a uma diminuição da morte celular programada nas áreas interdigitais, o que resulta em fenótipos de sindactilia (os dedos permanecem visivelmente unidos por uma membrana). A geração deste fenótipo é precedida pela inibição da expressão de genes envolvidos no processo apoptótico, tais como *snail*, *msx2*, *bambi* e *fgf10*, o que mostra que a actividade de ERG está directamente ligada à transdução de sinal nas vias de BMPs e FGFs. Assim, a acção de ERG é imprescindível no desencadear do processo apoptótico desde estádios muito iniciais da indução da morte celular.

A relação de *erg* com as diferentes vias de sinalização génica envolvidas no desencadeamento do processo apoptótico - tais como a de FGFs, BMPs e Ácido Retinoico (RA) - foi também clarificada. Experiências de ganho de função utilizando microesferas embebidas nestas moléculas mostram que estas três vias de sinalização regulam a expressão de *erg*. Em particular, a sinalização por BMPs activa a expressão do mesmo. Pelo contrário, o bloqueio destas moléculas não resulta na inibição de *erg*. Estes dados sugerem que adicionalmente à sinalização via BMPs, existirá uma outra cascata genética a induzir e/ou manter a expressão de *erg*. Mas, mais importante, este estudo mostra que *erg* é um intermediário fundamental no estabelecimento das áreas de morte interdigital durante o desenvolvimento dos dedos, precedendo o começo da apoptose. Em conjunto, os resultados deste trabalho apoiam um modelo no qual ERG é responsável pelo destacamento celular e consequente indução de morte celular programada nas áreas interdigitais.

Para além do controlo do destacamento celular através da activação do gene *snail*, uma outra função essencial do ERG na apoptose poderá ser a inactivação da expressão de *fgf8* na ectoderme distal do interdígito, dado que a inibição da actividade do ERG leva à manutenção da expressão do *fgf8* distalmente.

No entanto, é necessária a realização de mais experiências para clarificar, nomeadamente, a indução da expressão de *erg* através de BMPs e Ácido Retinóico. Uma possível abordagem seria a inibição conjunta de um ou vários elementos destas vias de sinalização de forma a esclarecer quais os elementos que actuam de forma conjunta para a indução e/ou manutenção da expressão de *erg*. Seria também importante melhorar a electroporação interdigital de RNAi para conseguir a perda de função na maior parte do mesênquima interdigital, tal como a realização de *western blots* de maneira a comprovar que a proteína não é traduzida. Ao mesmo tempo, seria de grande interesse a clonagem da sequência completa de *erg* para estudos de sobreexpressão no autopódio, confirmando-se assim se o aumento da sua actividade poderia induzir morte celular ectópica.

Palavras chave: Canal de potássio ERG, apoptose, desenvolvimento dos membro, sinalização por FGF e BMP

Table of Contents

I. Introduction

Vertebrate limb development

The vertebrate limb has been an important developmental model for the study of programmed cell death during embryogenesis since its apoptosis pattern is a consistent component in limb morphogenesis (Zuzarte-Luis and Hurle, 2005).

The early limb primordium of the amniota embryos is a simple structure. It starts as a core of mesenchymal cells encompassed by ectoderm and appears as a bud growing on restricted areas of the lateral plate mesoderm (LPM). These areas, called limb fields, are subjected to the influence of a cross-talk of genetic signaling cascades (*wnt* and *fgf*) between the LPM and ectoderm above. Wnt-stabilized FGF10 at LPM, activates FGF8 in the AER progenitors, which results in the establishment of an epithelial–mesenchymal feedback loop between AER-secreted FGF8 and mesenchymal FGF10 (Kawakami *el al*, 2001). The mesodermal cells of the early limb bud have skeletogenic potencial but are maintained undifferentiated and proliferating by the influence of a thickened region of the ectoderm at the distal margin of the bud, the apical ectodermal ridge (AER) (Kawakami et al., 2001; Montero and Hurle, 2010).

The vertebrate limb bud development is controlled by three signaling centers, the apical ectodermal ridge (AER) a specialized thickened region of the ectoderm at the distal margin of the limb bud, the polarizing region (ZPA) in the posterior mesenchyme and the non-ridge ectoderm. These signaling centers produce instructive signals that coordinately control proximo-distal (PD), anterior-posterior (AP) and dorsal-ventral (DV) limb axis formation. In particular, the ZPA produces Sonic Hedgehog (SHH), the dorsal ectoderm secretes WNT7a (Dealy et al., 1993; Parr et al., 1993), while the AER produces several fibroblast growth factors (FGF8, FGF4, FGF9, FGF17), FGF8 being the one of most importance. These signals from the AER act on the subjacent mesodermal cells that constitute the progress-zone (PZ), keeping them in a proliferative and undetermined state. According to the progress-zone model, the cells identities are determined along the PD axis by a ‘clock-type’ mechanism as they leave the progress zone, so the cell identities depend on the time of exit (Saunders J. W., 1948.; reviewed in (Zeller et al., 2009). Differentiation into cartilage, and cell death, occur when the cells of the PZ become displaced proximally into the core of the bud. More recently, the differentiation-front model assumes that PD identities are determined when the mesenchyme stops being under the AER-FGF signaling domain, when the proliferating mesenchyme leaves the undifferentiated zone (Tabin and Wolpert, 2007). On the other hand, it has been proposed the two-signal model whereas retinoic acid (RA) and FGF signaling induce proximal and distal cell fates in the limb bud mesenchyme, respectively. (Mercader et al., 2000). This hypothesis was analyzed during chicken limb bud development and has shown that RA induces proximal cell identity in the limb bud

mesenchyme by the induction of *meis1* and *meis2* expression, whereas AER-FGFs, which antagonize RA signaling, induce distal cell identity by the activation of *hoxa11* and *hoxa13*.

During the progression of limb bud development, the three signaling centers are interlinked by an epithelial-mesenchymal (e-m) feedback loop that functions to propagate both AER-*fgf* and ZPA-*shh* expression. This e-m feedback loop is established by transcriptional upregulation of *gremlin1* (the bone morphogenetic protein (BMP) antagonist) in a subpopulation of SHH responsive cells located in the dorsal and ventral part of the distal limb bud mesenchyme (Zeller, 2010).

Digit development

During limb bud development, cells that leave the PZ can undergo chondrogenesis and form the cartilage template for the skeleton or can die by apoptosis, defining regions of cell death around these chondrogenic aggregates (reviewed in Montero and Hurlé, 2010).

Physiological cell death is a key mechanism that ensures appropriate development and maintenance of tissues and organs in multicellular organisms. Cell death plays a role in sculpting the tetrapod limb that is crucial for the determination of its final shape and skeletal pattern. The involvement of cell death in vertebrate limb morphogenesis appears to be a characteristic of the amniotes only and exhibit significant differences between species (Hurle et al., 1996; Zuzarte-Luis and Hurle, 2002). The death (or lack of it) of specific cells in the vertebrate limb is genetically programmed and has been selected over the course of evolution (Gilbert, 2006). Cell death occurs in well-defined domains and sculpts the shape of the limb, eliminating the undifferentiated mesodermal cells (Zuzarte-Luis and Hurle, 2005) located between the differentiating cartilages (Hurle et al., 1996). Indeed, cell death is essential if joints are to form and fingers are to become separate (Gilbert, 2006). In the early stages of the avian limb development, the anterior (ANZ) and posterior (PNZ) necrotic zones eliminate the mesodermal cells located anterior and posterior to the zone of formation of the proximal skeletal components of the limb (Figure 1) (Montero et al., 2001). Another area of cell death is the opaque patch (OP) and takes place in the central mesenchyme of the limb, between the zeugopodial cartilages (Zuzarte-Luis and Hurle, 2002) (Figure 1). At more advanced stages of development, elimination of interdigital cells between the developing digits occurs in the interdigital necrotic zones (INZ) (Montero et al., 2001). In species with webbed digits, such the duck, apoptosis is limited to the distal part of the interdigit. Also, in species with autopods of singular morphology, for example the coot (*Fulika atra*) which have digits with lateral membranous lobulations or the splitted autopod of the chameleons, the pattern of interdigital cell death correlates closely with the specific phenotype of each species (Zuzarte-Luis et al., 2004). Although these zones are referred to as 'necrotic', this term is a holdover from the days when no distinction was made between necrotic death and apoptotic cell death (Gilbert, 2006).

Individualization of the digits is progressively achieved partly through the morphogenetic role of interdigital cell death (ICD) (Saunders and Gasseling, 1962). The current model supposes the

formation of an interdigital tissue that subsequently degenerates and, as a result, digits individualize. Under this model, ICD would restrict the growth of the interdigital tissue. However, sculpturing the limb by interdigital tissue removal (as occurs in reptiles, birds, and mammals) is not the only way of making free digits, as exemplified by the amphibian forelimb, where the digits form by differential growth without participation of cell death (e.g., as demonstrated in Xenopus by (Fallon and Cameron, 1977)). In amniotes, differential growth also participates in the separation of the digits (Salas-Vidal et al., 2001). Therefore, both cell death and cell proliferation are crucial processes during the morphogenesis of the digits (Fernandez-Teran et al., 2006).

Figure 1 – Representation of the anterior necrotic zone (ANZ), posterior necrotic zone (PNZ), opaque patch (OP) and interdigital necrotic zone (INZ). Courtesy of Doctor Joaquín León.

In the chicken embryo, proper interdigital cell death at the INZ is first detected at stage 29–30HH (Hamburger and Hamilton, 1951) in the proximal part of the first, second, and third interdigital spaces, then in its distal part. Proximal and distal clusters of cell death in the interdigital spaces are first separated but later joined together and the whole interdigit exhibits massive cell death (Pautou, 1974). The INZ reaches its maximum at stage 31HH (day 7 and a half of incubation) and subsequently progressively declines (Fernandez-Teran et al., 2006).

Several experimental approaches have shown that the interdigital mesoderm contains cells with chondrogenic potential and when cell death is inhibited and chondrogenesis is activated, they are able to form an extra digit (Merino et al., 1999a).

The tissue components of the interdigit establish complex interactions through the production of a variety of secreted signaling molecules that control cell fate and tissue differentiation. Several molecules have been indentified that participate in the regulation of ICD; however, very little is known about their mechanism of action and how they interact and contribute to trigger interdigital cell death (Hernandez-Martinez et al., 2009).

Molecular regulation of Interdigital Cell Death

BMP, FGF, RA and Wnt signaling

Programmed cell death during limb development shares many control mechanisms with proliferation and differenciation. Depending on mesodermal cells differentiation status, the response to the same protein may have opposite effects. The bone morphogenetic proteins (BMPs), members of the transforming growth factor superfamily, known to be involved in chondrogenesis were identified as the triggering apoptotic signals for both the ectoderm of the AER and mesodermal cells. The undifferentiated limb mesoderm undergoes apoptosis when is exposed to BMPs, but if the cells have initiated aggregation into the prechondrogenic blastemas, BMPs induce chondrogenesis (Ganan et al., 1996; Montero et al., 2001). It is interesting that factors responsible for the growth and differentiation of the skeleton are also the triggers for the apoptotic process (Zuzarte-Luis and Hurle, 2005). Several members of the BMP family (BMP-2, BMP-4, BMP-5 and BMP-7) are expressed in the undifferentiated limb mesoderm, AER and in the interdigital mesenchyme, coincident with apoptotic areas (Merino et al., 1999b). BMPs exert their function through serine/threonine receptor kinases composed of type I and type II receptors. The type IA and IB receptors mediate the chondrogenic effect of BMPs while the receptor implicated in the control of apoptosis awaits clarification (Figure 2) (Zuzarte and Hurle, 2005). There are at least two BMP intracellular signaling pathways through which BMPs exercise their apoptotic effect. Ligand binding of BMPs to their receptors activates members of the SMAD family. SMAD 1, 5 and 8 are phosphorylated coassembled with a cofactor, SMAD 4, and translocated into the nucleus where they activate gene transcription. The other pathway involved in apoptosis is the mitogen activated protein kinase (MAPK) pathway (Figure 2) (Montero *et al*, 2001; Zuzarte-Luis and Hurle, 2005). BMP activity is spatially and temporally fine-tuned by other factors during limb development such as antagonists of BMP function like Gremlin, Chordin and Noggin (Capdevila et al., 1999; Francis-West et al., 1999; Merino et al., 1998; Merino et al., 1999b). These antagonists share the functional property of binding specifically to BMPs, preventing their interaction with their receptors. This way, the function of BMPs is regulated specifically by different BMP antagonists that act in a complementary fashion rather than being redundant signals (Merino et al., 1999b). Gremlin for instance, is very important in limb patterning since it moderates BMP inhibition of FGFs, allowing the maintenance of the signaling loop between the ZPA (*shh*) and the AER (*fgf*) (*fgf-shh* feedback loop) (Khokha et al., 2003). Gremlin also regulates the regression of the interdigital tissue in the duck since it is expressed in a pattern covering the whole interdigital space except the most distal mesenchyme where cells will die by apoptosis (Merino et al., 1999b).

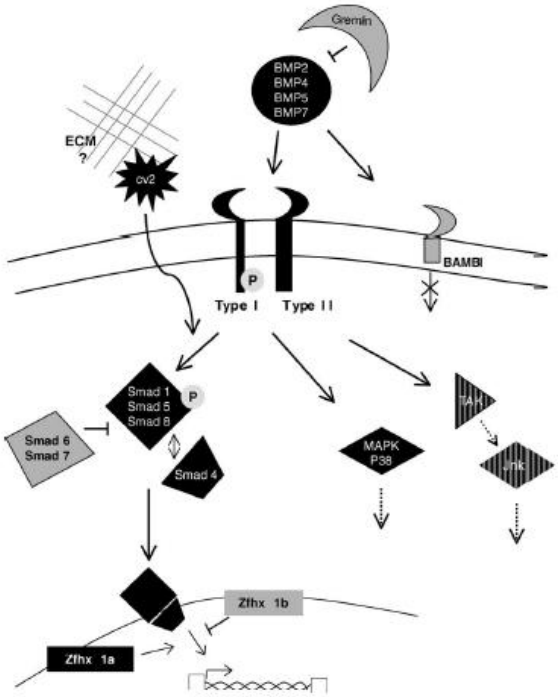

Figure 2 – Schematic representation of BMP signaling pathway involved in interdigital cell death triggering. Inhibitory molecules are colored in grey. Active signaling molecules are colored in black (From Zuzarte-Luis et al., 2005).

In this context, Montero and colleagues (2001) showed that BMPs alone are not sufficient to trigger the apoptotic process during limb development, since blockage of FGF signaling through application of its inhibitor SU5402 inhibited physiological and exogenous BMP mediated apoptosis. Delivery of exogenous FGFs strongly increased cell death 24 hours after the application. This shows that FGF signaling is also necessary for apoptosis and that the establishment of the areas of cell death is regulated by the convergence of FGF and BMP-mediated signaling pathways (Montero et al., 2001).

It has been shown by Hernández-Martínez and colleagues that growth to form mouse and chick interdigital tissue occurs within a 12 hour time window. It has been proposed that most interdigital cells derive from the distal mesenchyme, which survival depends on ectodermal FGF8, and are the ones fated to die. According to this model, cell death is initiated in the distal region and as the limb grows and interdigital regression occurs, the dying cells acquire a more proximal position. This explains a progressive process rather than massive mechanism of cell death, through which mouse and distal chick ICD occurs. Chick's most proximal ICD appears to follow a different mechanism dependent on interdigital BMP activity. Recently, it has been showed that modulation of Wnt/β-catenin signal in the limb ectoderm including the AER regulates interdigital apoptosis. They also demonstrated that ectodermal Wnt/β-catenin signaling can positively regulate *fgf8* possibly antagonizing the BMP signaling within the AER (Villacorte et al., 2010).

Caspase activation

Apoptosis takes place by the action of cysteine-aspartic acid proteases, usually called caspases. There are at least two known pathways responsible for caspase activation, proteolysis and DNA fragmentation, and consequent apoptosis: the extrinsic pathway (death receptor pathway) and the intrinsic pathway (mitochondrial pathway). The extrinsic pathway requires binding of ligands (like CD95, TNF-α or Fas-ligand) to specific transmembrane receptors belonging to the superfamily of the tumor necrosis factor receptors (TNF-receptors), followed by the activation of caspase 8 (and/or caspase 10). The intrinsic pathway is triggered by modifications in the permeability of the mitochondrial membrane followed by the release of cytochrome *c* from de mitochondrial matrix into the cytosol. The apoptosome is the central element of the apoptotic machinery of the intrinsic pathway and is constituted by the Apaf-1 together with caspase 9 and cytochrome *c*. Both pathways involve the activation of initiator caspases (caspase 8 and caspase 9 specific of the extrinsic and intrinsic pathway respectively) by proteolytic cleavage of their pro-domain. After several intermediate steps, the two pathways converge in the activation of the effector caspase 3, caspase 6, and caspase 7, which are proteases responsible for cell degradation. Still, the pathways are also not mutually exclusive of each other, they can be interconnected at different levels. For example, the activation of caspase 8 in the death receptor pathway may induce the formation of proapoptotic proteins of the Bcl-2 family (Bax, Bag, Bak, Bcl-xs), which translocate to the outer mitochondrial membrane and facilitate the extrusion of cytochrome *c*, aggravating the apoptosis process. The apoptosis-inducing factor (AIF), a factor that is also released from the mitochondria, can also trigger apoptosis without caspases involvement (Burg et al., 2006; Zuzarte-Luis and Hurle, 2005). Also, it has been reported that even when caspases are fully inhibited, interdigital cell death in mouse embryos still occurs by a caspase-independent pathway (Chautan et al., 1999). Caspase 3 has been proposed to be the major effector caspase during physiological cell death in the developing limb. Even though, when the limb bud is treated with specific caspase 3 inhibitor peptides, apoptosis is only reduced and not blocked (Huang and Hales, 2002). Which of the pathways operates in the activation of caspase 3 by the dying cells of the developing limb is still a matter of debate (Zuzarte-Luis and Hurle, 2005). The molecular cascade responsible for the execution of apoptosis remains largely unknown (Zuzarte-Luis and Hurle, 2005). Besides the morphological features of apoptotic cells, apoptotic volume decrease (AVD) due to efflux of K^+, Cl^-, and H_2O is an early hallmark of apoptosis that occurs within the 1^{st} and 4^{th} hour after apoptosis induction (Burg et al., 2006). This corresponds to the initial phase of AVD that takes place before the activation of the apoptosome. The late phase of AVD includes the subsequent caspase activation that leads to DNA fragmentation (Burg et al., 2006).

Electric fields in development

In addition to the numerous genetic cascades known to be involved in the induction and outgrowth of the vertebrate limb, there are epigenetic mechanisms that influence the pattern, closing the loop between the nucleus and its environment. One of the epigenetic mechanisms suggested for limb bud initiation imply an endogenous electric field. Altizer and colleagues (2001) found an outwardly directed, steady, ionic current before and during the emergence of the mouse and chick limb bud. On the other hand, in the flank regions in the dorsal-ventral plane of the limb bud, the currents were usually inwardly directed (the direction of Na^+ uptake by ectoderm), fulfilling a direct current circuit. The same type of mechanism was also observed in Borgens work regarding the amphibian limb development. When the endogenous ionic current of the limb field was reversed in stage 13HH (from Hamburger and Hamilton, 1951) chick embryos, for approximately 6 hours, limbs with skeletal pieces missing, shortened or thickened were formed. This abnormal limb development supports the existence of an early physiological (electrical) control of limb development, required for the normal development of the bud (Altizer et al., 2001). Deregulated transmembrane ion flow via ion channels has been implicated in the initiation and progression of apoptosis (Burg et al., 2006). After gene ontogeny analysis of limb bud transcriptome (Affymetrix DNA chips) of embryonic mouse limbs, ERG channel, an outward K^+ channel, was found to be one of the most strongly expressed ion transporter in this tissue (Margarida Santos thesis).

Potassium channels and cell death

Potassium (K^+) channels are one of the most diverse classes of membrane proteins and are ubiquitously found in many cells types (Felipe et al., 2006). Kv channels are characterized by their sensitivity to membrane potential. They open upon membrane depolarization, enabling K^+ efflux based on its electrochemical driving force ($[K^+]in$ >> $[K^+]out$), causing membrane hyperpolarization. The properties of Kv currents are diverse due to association of the pore-forming α subunits with modulatory βsubunits and alternative splicing of primary transcripts. There are twelve Kv subfamilies (Kv1-Kv12). The Kv channel α subunits have six transmembrane domains (S1–S6) and cytoplasmic N- and C- termini (Burg et al., 2006; Felipe et al., 2006). Besides the morphological features of apoptotic cells, apoptotic volume decrease (AVD) due to efflux of K^+, Cl^-, and H_2O is an early hallmark of apoptosis that occurs within the 1st and 4th hour after apoptosis induction (Burg et al., 2006).

Biological activity of ERG *ether-a-go-go* (eag) family of voltage-dependent channels

ERG channels are encoded by three different genes: *erg1, erg2* and *erg3* and belong to the *ether-a-go-go* (eag) family of voltage-dependent channels. They are known to be involved in the action potencial timing and have been well characterized as the molecular basis of the cardiac repolarizing current. Point mutations of the human *erg1* gene (hERG also known as Kv11.1) cause the hereditary Long-QT syndrome or chronic arrhythmia (Greenwood et al., 2009; Scholz et al., 2009) It has been

proposed by Cherubini and colleagues a model for regulation of β1-integrin signaling by hERG channel activity, in which hERG channels are physically coupled to β1-integrin and represent a key step in integrin-regulated downstream signaling (Cherubini et al., 2005).

When limb fields start to appear (stage 18HH), *erg* expression pattern is restricted to the presumptive forelimb and hindlimb field region. At the anterior region of the embryo *erg* expression is seen in the myogenic precursors that derivate from the somites, and at the posterior region of the embryo to the medial part of the somites. As development continues, *erg* expression becomes stronger at the most distal part of the limbs, and by stage 23HH is restricted to the dorsal and distal regions of those. At stage 26HH, embryos express *erg* in both anterior and posterior necrotic zones, and by stage 30HH in the interdigital necrotic zone as well as in the medial part corresponding to the differentiating cells.

Objectives

Due to the strong co-expression of *erg* gene with apoptotic areas and previous evidence of the influence of ionic currents in limb induction and outgrowth (Altizer et al., 2001), we aim to further analyze the relationship of this gene with others gene cascades known to be involved in the control of apoptosis in limb development and this way understand the regulation of *erg* during digit patterning. For that we will study the expression pattern of *erg* during the establishment of the INZ during digit development. We will also depict the relationship of *erg* activity with different signaling molecules involved in the induction of programmed cell death. Also, we will study how *erg* controls the expression of key player in the apoptotic process. To understand if the role of *erg* is conserved in different organisms we will use two different species in this work, one with free digits, the chicken, and the other with webbed digits, the duck.

II. Materials and Methods

The composition of the solutions underlined is detailed in *Appendix I – Buffers, Solutions and Media.*

II.1 Animal models

In the field of experimental embryology, the avian embryos, namely the duck and chick, have been a good experimental models for studying developmental events because of their ready availability, they allow the manipulation of high numbers of embryos (fertilized eggs), and they are amenable to embryological and surgical manipulations at the desirable stages of development. Also, the chicken and duck are model organisms especially advantageous for this type of studies compared to other animal models due to the easiness to realize gain and loss-of-function experiments through transient transfection methods (Odani et al., 2008; Sauka-Spengler and Barembaum, 2008). These techniques allow transient spatiotemporally targeted gene alterations, making possible to study the effects of gene inactivation or overexpression on downstream transcriptional regulation and on embryonic derivatives (Sauka-Spengler and Barembaum, 2008). These species are also well characterized in terms of genes associated with programmed cell death and present a different apoptotic pattern in the interdigit, important in the ambit of this study (Merino et al., 1999b).

II.2 Embryo collection, fixation and storage

White legorn chicken (*Gallus gallus*) and duck (*Anas platyrhynchos*) fertilized eggs were acquired from *Sociedade Agrícola da Quinta da Freiria, S.A.*. Chicken embryos were staged according to the Hamburger and Hamilton developmental table (Hamburger and Hamilton, 1951) (see Appendix V).

We used chick embryos between 68-72 hours and 9 days of incubation, stage 19HH (just before the appearance of the apoptotic areas during limb development) to stage 35HH (when the interdigital mesodermal cells regression ceases) and duck embryos between 7 and 10 days of incubation. The fertilized eggs are incubated at 40% humidity and 37.5-38°C until the required embryonic stage.

To ensure that the embryos were maintained in an RNAse free environment and in aseptic conditions, all microsurgery instruments were sterilized at 120^{o}C. Chicken and duck eggs were windowed when embryos reached the desired stage of development. The embryos were dissected from the yolk/viteline sac, and transferred to a sterilized petri dish containing Phosphate buffer saline (PBS). From stage 26HH onwards only the hindlimbs were collected for further analysis. Then the embryos were fixed in 4% paraformaldehyde (PFA) to preserve embryo structures and to prevent mRNA degradation. This fixation occurred at 4^{o}C for 2 hours or overnight (ON) depending on the following protocol, immunostaining or *in situ* hybridization assay, respectively. Next, embryos were washed twice in a PBT solution in order to permeate the tissues and were dehydrated through a crescent series of methanol in PBT (25%, 50%, 75% and 100%) and stored at -20ºC in order to stabilize RNAses and prevent transcript degradation. It is important that the embryos are stored in

absolute methanol to avoid water crystals that could compromise the tissues integrity. (with exception of the embryos for immunostaining in sections, that are not dehydrated and follow the histological protocol described bellow (see section II.6)

II.3 Experimental manipulation of the limb

Before starting any manipulation process, eggs were withdrawn from the incubator about 1 hour in advance in order to slow down embryo heart beating and decrease their blood pressure. This was done to induce a faster healing process in case of vessel injury during manipulation.

Both bead implantation and electroporation experiments were performed *in ovo*, and for that we incubated eggs with their blunt pole up. This way, the air chamber localized at the top of the egg and the embryo was accessed performing a window in the eggshell without touching the embryo. After that, the vitelline membrane was carefully opened at the site of manipulation using fine forceps. In all cases, the right hindlimb was manipulated and left hindlimb was employed as a control.

II.3.1 Bead Implantation

The function of the *erg* gene and its regulation by other molecules known to be involved in the apoptotic process was studied by analyzing the effects of local application of different molecules through bead implantation.

Beads were implanted at stage 28-29HH (Hamburger and Hamilton, 1951) chicken embryos, into the third interdigital space at its most distal tip, subjacent to the AER. For this purpose the eggs were windowed, the vitelline membrane was opened with fine forceps and the right limb bud was exposed. Next, a little incision was made on the distal part of the third interdigital space and the bead was inserted into the limb mesoderm. For this experiment we used heparin acrylic beads (Sigma, H5263) soaked in BMP2 (0.5µg/µl), BMP4 (0,1 µg/µl), Noggin (1µg/µl), Gremlin (1µg/µl), FGF8 (1µg/µl), FGF10 (1µg/µl) (all from R&D systems) or ERG inhibitor (M5060 E-4031 Sigma) (10mM) and ion exchange (AG1-X2, Bio-Rad) beads soaked in SU5402 (2 µg/µl, Calbiochem), retinoic acid (50µg/µl) or Citral (25% in DMSO, Fulka). In all the experiments PBS-soaked beads were also implanted as a control. We selected beads ranging between 100 and 200µm in diameter. The heparin acrylic beads were washed in PBS and incubated for 1 hour at room temperature in 2µl of the selected protein solution. The AG1-X2 beads used for RA delivery followed a different protocol, in the dark. Beads were added to a microtube with 50-100µl of the retinoid solution and were vortexed for 30min. After that, the beads were spin down and the retinoic solution was substituted by 100µl of Dulbecco's medium and mixed for 10min. Finally the supernatant was removed and the beads were resuspended in 20µl of cell medium.

After bead implantation the egg was sealed with tape to prevent contaminations and re-incubated until the embryo reached the desired stage.

In order to continuously deliver the ERG inhibitor, several beads were implanted in the same embryo at different times. The first bead was implanted at stage 28-29HH, and 6 to 7 hours later a second bead was implanted distally. In the next 12 hours period a third bead was implanted. Embryos were then fixed at different time points for ulterior processing.

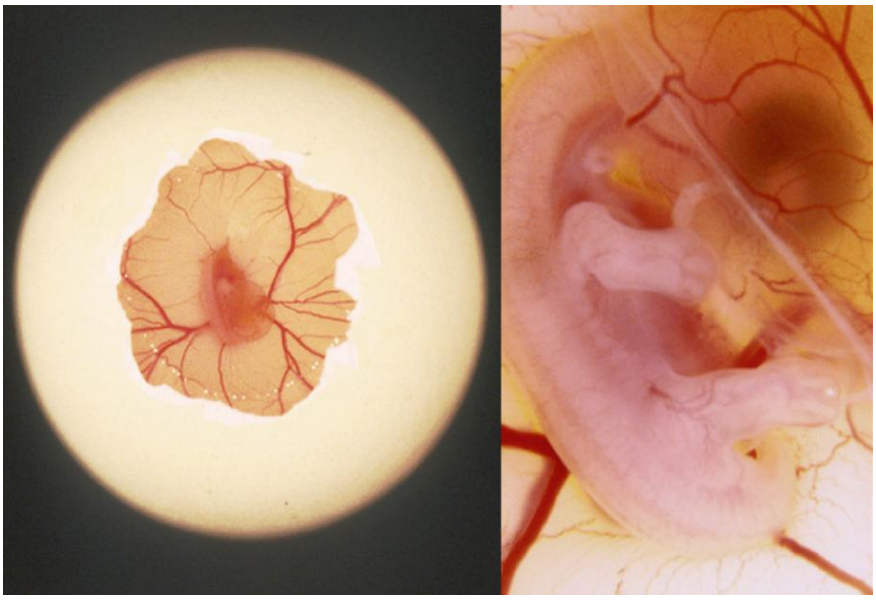

Figure 3 – Experimental manipulation of a chicken embryo, *in ovo*. (A) *In ovo* manipulation of a chicken embryo by opening a window in the eggshield. (B) Application of beads in the third interdigital space *in ovo*. Courtesy of Doctor Joaquín León.

II.3.2 *erg* RNAi electroporation

The electroporation method involves the application of an electric field to a tissue that transiently disrupts the stability of the cell plasma membrane. This results in the formation of small reversible pores through which entrance of DNA is allowed.

We used the pSUPER vector to drive the synthesis of RNAi transcripts that target specific mRNAs and suppress endogenous RNA activity. The RNAi against *erg* was cloned with the forward primer 5' – GAT CCC CAT ACG TCA CTG CCC TCT ACT TCA AGA GAG TAG AGG GCA GTG ACG TAT TTT TTG GAA A – 3' and reverse primer 5' – AGC TTT TCC AAA AAA TAC GTC ACT GCC CTC TAC TCT CTT GAA GTA GAG GGC AGT GAC GTA TGG G – 3' (Figure 4).

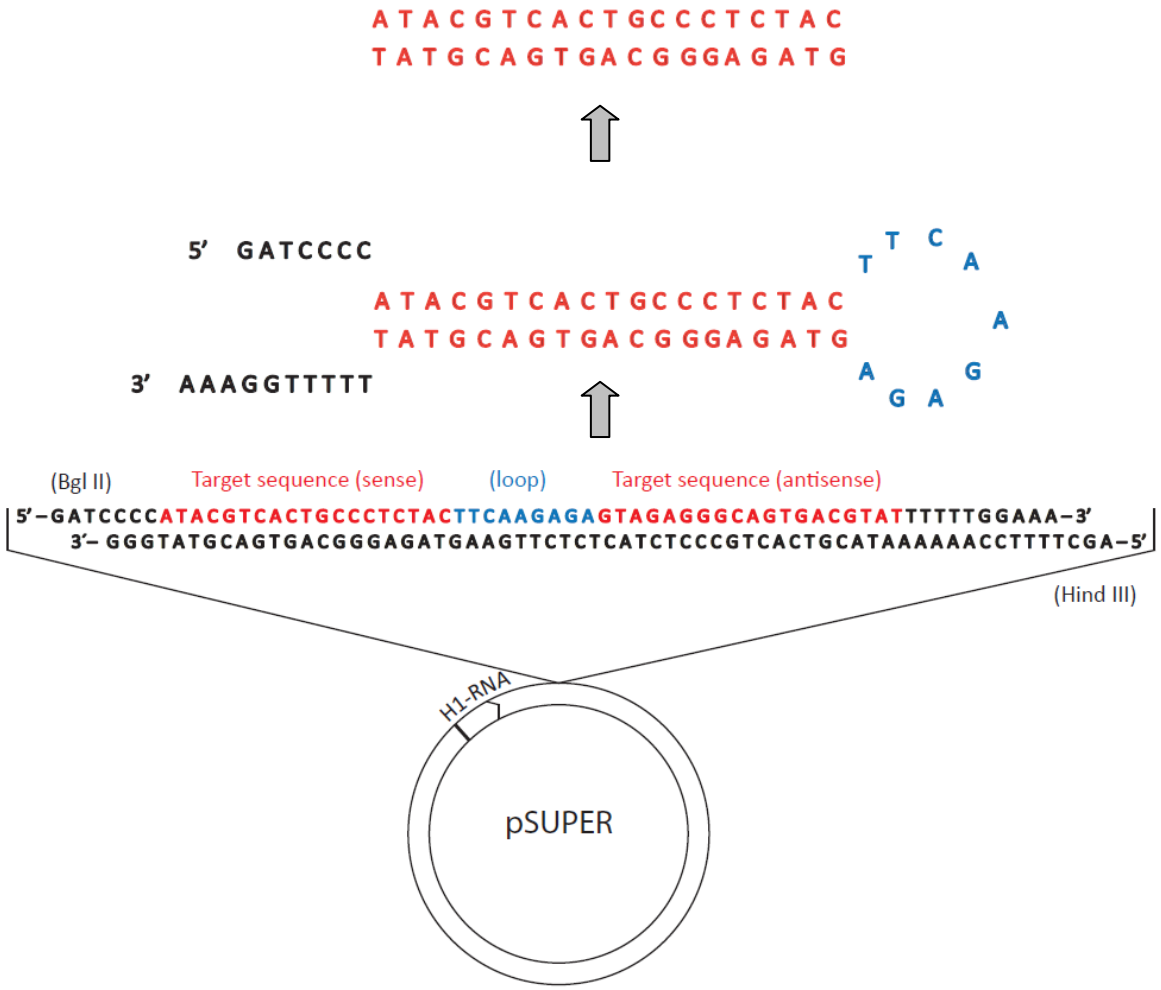

Figure 4 - Mechanism of synthesis of RNAi from the pSUPER vector.

Electroporation was done *in ovo*, at stage 28-29HH chick embryos. We microinjected into the third interdigit mesoderm a pSUPER-*erg* RNAi plasmid solution (5-6µg/µl) together with a pCAGGS-AGFP (0.5-1µg/µl) one that will be used as readout for cell transfection (Figure 3A). The solution also includes 5% of Fast green to contrast. Single electroporation of pCAGGS-AGFP at 5-6µg/µl was carried out as a control. Electroporation was performed using an Intracel TSS20 Ovodyne electroporator (Intracel LTD) using 5 pulses of 60 ms length (8 V each) with 50 ms interval. We placed the electrodes (cathode and the anode) on both dorsal and ventral sides of the right hindlimb, at the third interdigit level. Then we repeated the procedure with the electrodes in the inverse order to allow DNA transfection into the whole interdigit. (Figure 3B,C). After electroporation, eggs were sealed and re-incubated until the desired stage was reached.

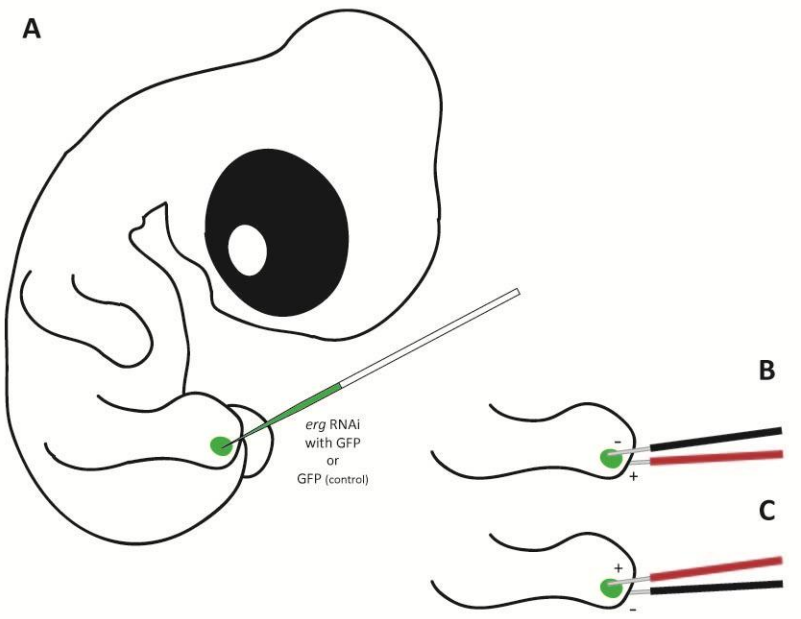

Figure 5 - Schematic representation of the electroporation technique. (A) injection of the DNA solution at the interdigital space. (B) and (C) positioning of the electrodes to perform electroporation.

II.4 Riboprobe preparation for whole-mount In situ hybridization

A chicken and duck *erg* cDNA fragments were available at the laboratory cloned into pGEM-T easy plasmid. RNA probes were synthesized from those plasmids using the restriction and RNA polymerase enzymes that are described in Table I.

First, the plasmid vector containing the cDNA of the gene of interest was linearized and purified. Linearization was done in two different settings in order to generate templates for both antisense (positive probe) and sense (negative control probe) probes. After digestion the DNA was purified by phenol:chloroform extraction (see next item in this section), and precipitated with ethanol (see below in this section). After drying, the pellet was resuspended in milliQ water.

Sequencing reaction

After plasmid purification, all sequences of cDNA of interest were checked. The primers used in the sequencing reaction annealed to RNA polymerase promoters T3, T7 or SP6 that flank the multiple cloning site of the vector (see Table I). Each 10µL reaction contained 2µL of BigDye® terminator sequencing buffer (5X), 2µL BigDye® terminator ready reaction mix, 500ng of template DNA and 5pmol of primers. The PCR conditions were the following:

Temperature	Time	
96ºC	1 min	
96ºC	10 sec	25 cycles
50ºC	5 sec	
60ºC	4 min	
4ºC	Until ready to purify	

After the PCR, the reaction product was precipitated. After mixing, the tubes were incubated at room temperature for 30min and centrifuged at 14000rpm for another 30min at 4ºC. The supernatant was removed and the pellet was washed in 250µL of 70% ethanol. The tubes were centrifuged at 14000 rpm for 15min at 4ºC. The supernatant was again removed and the pellet was air-dried. The samples were then sent to the IGC sequencing service. The resulting output sequences were analyzed in detail by the combined use of the BLAST (http://www.ncbi.nlm.nih.gov/BLAST/), Bioedit, Chromas and Sequence Analysis software.

cDNA	Plasmid	Restriction enzyme		RNA polymerase	
		sense	antisense	sense	antisense
c erg	pGEM-t easy	NcoI	Sal I	Sp6	T7
d erg	pGem-t easy	NcoI	BamH I	Sp6	T7
smad8	pCRII-TOPO	EcoRV	HindIII/BamH I	T3	T7
msx2	pBluescriptII SK (+/-)	HindIII/EcoRV	Spe I	T3	T7
snail	pBluescriptII SK (+/-)	XhoI	HindIII	T7	T3
bambi	pBluescriptII SK (+/-)	SacI	XbaI	T3	T7

Table I - Plasmids for the synthesis of riboprobes and the enzymes used for digestion and RNA polymerization.

II.4.1 Plasmid Linearization

Plasmidic DNA was digested with a unique restriction enzyme upstream in order to create a linear fragment. To obtain the template cDNA for probe transcription, we digested 10µg of the plasmidic DNA containing the cDNA of interest using 1µL of the appropriate restriction enzyme (see Table I),

2µL of the respective enzyme buffer (10x) and milliQ water for a final volume of 20µL. The reaction occurred for about 3 hours at 37°C. Completed digestion was confirmed by running 1µl of digestion product in a 0.8% agarose gel and observing a linear band with the total plasmid size. The linear plasmid was then purified by phenol:chloroform extraction and precipitated with ethanol.

Agarose gel electrophoresis

Agarose was dissolved in 1X TAE, usually at a concentration of 0.8%. Ethidium bromide was added in order to visualize the DNA with the use of a UV light to a final concentration of 0.2µg/mL. Loading buffer was added to each sample to a 1x final concentration and a DNA ladder was used to estimate the size of the DNA fragments. An electric current of 80-110V was applied to the gel immersed in 1X TAE buffer.

II.4.2 Phenol:Chloroform extraction

When the digestion reaction was completed the DNA was purified by phenol-chloroform extraction. This was performed to remove proteins from the nucleic acid solution. For this, milliQ water was used to make a final volume of 100µL to reduce the loss of DNA during the process and an equal volume of phenol-chloroform was added. The sample was mixed by strong vortexing and centrifuged for 5min at 14000 rpm. The DNA was recovered from the aqueous phase and transferred into a clean microtube and precipitated with ethanol.

II.4.3 RNA/DNA precipitation with ethanol

The nucleic acids were precipitated with 0.1 volumes of 3M sodium acetate (pH5.2) in the case of DNA or the same amount of lithium chloride for RNA samples, and 2.5 volumes of absolute ethanol for 30min at -80°C. The precipitated RNA/DNA was recovered by centrifugation at 14000rpm for 30min at 4°C. Then supernatant was disposed and the pellet was washed with 5 volumes of 70% ethanol by centrifugation at 14000rpm for 15min at 4°C. Finally, the supernatant was discarded and the RNA/DNA pellet was air-dried. The precipitated RNA/DNA was resuspended in 20µL of milliQ water and stored at -20°C.

II.4.4 *In vitro* DIG-labelled anti-sense RNA probe transcription

Riboprobes were synthesized by *in vitro* transcription with an adequate RNA polymerase and a mixture of dNTPs that contains DIG-labelled dUTPs. The synthesis of DIG-labelled anti-sense RNA probes was carried out by in vitro transcription at 37°C for 2h 30 min in a 20 µl reaction. The reaction contained 1X transcription buffer, 20U of RNase inhibitor, 1X DIG RNA labelling mix (Roche), 20 U of the appropriate RNA polymerase and 1 µg of the linearized template. After the generation of the riboprobe, 1 µl of the mixture was run on an agarose gel to estimate the amount of the probe.

Afterwards, the RNA was precipitated with ethanol, resuspended in 20 µl of milliQ water and stored at - 20°C.

II.5 Whole-mount *In situ* hybridization

The *in situ* hybridization technique was used to detect specific messenger RNA (mRNA) sequences in intact cells or tissues. It consists in the use of a single-stranded gene-specific RNA probe (riboprobe) labelled with an epitope, in this case digoxigenin (DIG). The riboprobe will only bind to its complementary mRNA transcripts, allowing the detection at the target gene expression sites. This allows great specificity considering that RNA/RNA hybrids are thermodynamically very stable and that hybridization is performed at stringent conditions (high temperature and increased content of formamide). The DIG-labeled RNA was detected by an anti-DIG antibody coupled to alkaline phosphatase (AP) and hybridization was visualized by a permanent dye that precipitates using BM-purple. (Veeck and Dahl, 2010).

The protocol was carried through for at least 3 days and all the washing and incubation steps were performed with gentle agitation using a roller, except when the opposite was mentioned.

On the first day, fixed embryos were rehydrated through graded methanols in PBT (100%, 75%, 50% and 25% methanol) and washed twice in PBT for about 10min each step. Then the embryos were bleached in 6% hydrogen peroxide in PBT for 1hour, at room temperature to block endogenous peroxidase activity. After that, they were washed three times for 5min in PBT. In order to improve probe penetration into the tissue during hybridization, the embryos were permeabilized by treatment with 10µg/ml proteinase K at room temperature (without agitation). The incubation time with proteinase K varied with the stage of the embryo and the level of penetration that we wanted to achieve. To stop the reaction the embryos were washed with fresh prepared glycine in PBT. Since the embryos are fragile after proteinase K treatment, embryos were fixed 20 min in PBT containing 4% PFA and 0.2% of glutaraldehyde at room temperature. To remove the fixative the embryos were washed twice with PBT for 5min. Then, the embryos were pre-hybridized with hybridization solution for 2 to 3 hours at 68-70^{o}C. The high temperature and content of formamide in the hybridization solution increase the hybridization reaction stringency and therefore probe-target mRNA specificity, preventing non-specific hybridizations. Embryos were incubated overnight with hybridization solution with the probe (400-700 ng/ml) at 68-70°C.

On the second day, the probe was recovered and stored at -20^{o}C for further use. Embryos were washed in stringent solutions (at hybridization temperature, without agitation) to remove non-hybridized RNA. First were washed twice with post-hybridization solution I for 1 hour, followed by two 30min washes with solution III. The embryos were further washed in MABT and then incubated in the blocking solution for 2 to 3 hours at room temperature. Finally, the embryos were incubated in the blocking solution with an anti-DIG antibody conjugated with AP in a 1:2000 ratio, overnight at 4^{o}C to allow specific antibody binding to Digoxigenin.

During the third day of protocol, the embryos were washed in MABT with levamisole (an endogenous alkaline phosphatase inhibitor) at room temperature, renewing the solution every hour. Washing at this point is of great importance since unbound antibody has to be removed to obtain an efficient signal-to-noise ratio. In our case, we wash the embryos for 1 to 3 days, to reduce background as much as possible. Embryos were then washed at room temperature three times with NTMT for 10 minutes to create an alkaline medium that allows phosphatase activity present in the antibody. AFter that, embryos were incubated in the developing solution BM-purple (Roche) in the dark and at room temperature. BM-purple reacts with the antibody AP, resulting in the formation of a purple precipitate in the cells where target transcripts are localized. The appearance of the signal depended on the probe used and was checked by observing the embryos under the stereoscope. When a clear signal was observed the reaction was stopped with PBT. The embryos were fixed in 4% PFA overnight and stored in PBT until further analysis. As a control we performed the same protocol using a sense probe that didn't present precipitation. Results were imaged in a stereoscope attached to a digital camera.

Some of the embryos after *in situ* hybridization protocol were sectioned in a cryostat. For that, embryos previously soaked in sucrose solution were embedded in mounting medium for frozen samples and sectioned at 20 µm (see section II.6).

II.6 Histological analysis

II.6.1 Tissue processing and gelatin embedding

After proper embryo fixation (in 4% PFA at 4^{o}C for 2 hours for immunostaining/TUNEL assay, or after the whole-mount *in situ* protocol final fixation), the embryos were rinsed in PBS and soaked in 10% sucrose in PBS overnight at 4^{o}C. In the next day, embryos were washed in a fresh 10% sucrose-PBS solution and incubated in PBS with 10% gelatin and 10% sucrose at 37^{o}C for an hour. After this, embryos were transferred to a mould with an already solidified gelatin layer, covered with 37^{o}C 10% gelatin and oriented in the desired position. The mould was removed after gelatin solidification (at room temperature or 4^{o}C) and the gelatin block was cut in the appropriate size and orientation. The samples were fixed in a slice of cork with Tissue Tek O.C.T.™ Compound, frozen and stored at -80^{o}C until cryostat sectioning.

Samples were sectioned at 12-14µm for future immunostaing/TUNEL assay or at 20-24µm for embryos after *in situ* hybridization. Sections were collected in *SuperFrost Plus* slides for better adhesion, and stored at -20^{o}C.

II.7 Limb morphological analysis

II.7.1 Alcian green staining

The morphology of the limbs was initially analyzed in specimens stained for cartilage following alcian green protocol (Ganan et al., 1996). The embryos were sacrificed, fixed in 5% trichloroacetic acid overnight and stained with 0.1% Alcian green during the next night. In the following day, embryos were washed in an acid alcohol solution and dehydrated with absolute ethanol (2 washes of one hour each). Finally, the embryos were cleared in methyl salicylate.

II.8 Cell death analysis

The pattern of cell death was analyzed by using the TUNEL assay performed in tissue sections. Acridine orange was employed as an alternative to the TUNEL method in whole autopods.

II.8.1 Acridine Orange

The vital dye acridine orange permeates dying cells to bind chromatin and interacts with DNA and RNA by intercalation or electrostatic attraction respectively. DNA intercalated acridine orange fluoresces green (525nm). It has been shown in drosophila embryos that acridine orange, is specific for apoptotic forms of cell death and does not significantly label cells undergoing necrotic death provoked by injury (Abrams et al., 1993). The treated embryo legs were rinsed in 1:1000 acridine orange (1mg/ml stock solution) in preheated PBS and incubated at 37^{o}C for 20-30min. Next, the embryos were washed twice in preheated PBS for 5min each. After a final PBS wash at room temperature, interdigital cell death was visualized with a fluorescent stereoscope with a camera attached.

II.8.2 TUNEL analysis of dying cells

Cryopreserved tissue sections of autopods were analyzed for apoptotic DNA fragmentation by the terminal deoxynucleotidyl transferase-mediated dUTP-TRIC nick end labeling (TUNEL) assay, using the in situ cell death detection kit (Roche). Labeling of DNA strand breaks by Terminal deoxynucleotidyl transferase (TdT) which catalyzes polymerization of labeled nucleotides to free 3'-OH DNA ends in a template-independent manner (TUNEL-reaction). TMR red labeled nucleotides, incorporated in nucleotide polymers, are detected and quantified by fluorescence microscopy.

To evaluate the rate between living and dead cells, TUNEL was combined with DAPI (and/or TO-PRO3) staining and immunostaining for phospho histone H3 to detect proliferating cells. For that, we used longitudinal 14µm sections of the third interdigit. To remove the gelatin from the sections, the slides were washed/emerged in preheated (37^{o}C) TBS for 30-60min. The slides were washed three times for 5min in TBS and incubated for 30min in block buffer. This is important to inhibit the

unspecific ligation of the primary antibody to the cells. After blocking, the slides were incubated with 1:100 of the primary antibody against H3 (anti-H3, rat Sigma h9908) in TBS++, overnight at 4°C. In the next day, sections were washed three times for 5min in TBS++, followed by the incubation of the respective secondary antibody (goat anti-rat Alexa 488) for one hour, at 37°C. Next, slides were further washed with TBS three times, and incubated with DAPI (1:10000) for 10min to label the nucleus. After this, samples were washed with TBS once and incubated with TO-PRO3 (1:1000) for 15' and washed again with TBS. The sections were then fixed with 4%PFA for 50min at room temperature. After several TBS washes for about 2hours, sections were incubated with 0.2%triton 0.05%tween TBS for 30min and washed in TBS twice after. Next, slides were washed in 10mM Tris-HCl + 5mM EDTA for 5min and permeated with 20µg/ml proteinase K in 10mM Tris-HCl + 5mM EDTA for 15min at room temperature. Then, the slides were washed twice with 5mM EDTA for 5min followed by a 10min TdT buffer wash. Finally the slides were incubated with the TUNEL TMR kit (Roche) for 2 hours at 37°C. After incubation, slides were washed twice in SSC + EDTA for 10min and washed three times in TBS for 5min. Sections were once again contrasted with DAPI, washed in TBS for 5min and finally mounted in vectashield. The slides were stored at 4°C until further analysis in the fluorescent microscope.

II.9 Confocal microscopy

Samples were examined with a laser confocal microscope (Zeiss LSM 510 META) by using a Plan-Neofluar 10x or Plan-Apochromat 20x objectives, and argon ion laser (488nm) to excite FITC fluorescence and a HeNe laser (543nm) to excite Texas Red. For stacks digitalization and image processing, we used ImageJ software. The images shown in this study are the most representative of the experiment.

II.10 Statistic analysis

Interdigits of hindlimbs injected with *erg* RNAi+AGFP (n=75) or AGFP (n=38) constructs, and their respective control legs were measured using ImageJ software. Data was grouped in two sets, one for *erg* RNAi+AGFP and the other for AGFP controls, and two subsets, manipulated and controls. Sets were analyzed using the GraphPad Prism 5 software and statistic significance of the experimental procedure was evaluated using the non-parametric 2-tailed Wilcoxon matched-pairs signed rank test, with a 95% confidence interval.

III. Results

Expression of *erg* during limb development correlates directly with apoptosis

The expression pattern of *erg* was studied in chicken (*Gallus gallus*) embryos during digit development, between stages 28 to 35HH (Hamburger and Hamilton, 1951, see Appendix V).

Erg exhibited a dynamic pattern of expression in the limb mesoderm throughout all the studied stages (Figure 6 and 7). We have observed that interdigital mesenchymal cells showed a high level of *erg* transcripts at stages immediately preceding cell death. Well-defined domains of *erg* expression were detected in a pattern that correlates with the areas of limb cell death, in particular the interdigital necrotic zones (INZ). In the interdigital tissue, *erg* exhibits a pattern of expression prefiguring the areas of interdigital cell death (ICD) (Figure 6A-D and Figure 7) beginning at stage 27HH. Between stages 27HH and 30HH, *erg* transcripts were concentrated in the most proximal interdigital mesoderm (Figure 6A-D). From stage 31HH onwards, the most central interdigital expression of *erg* was gradually lost, becoming restricted to the tissue around the digits (Figure 6E-I and Figure 7). At these advanced stages of limb development, *erg* was progressively expressed in the perichondrium of the developing digits, surrounding the diaphysis (Figure 6I, black arrowhead), (Figure 6I, N and O) and in the remaining interdigit (Figure 6I).

This correlation between *erg* gene expression and ICD was also observed in the webbed digits of duck embryos, in which cell death is restricted to the most distal portion of the interdigital tissue (Hurle and Colvee, 1982) (Figure 8C, black arrowhead). During chick limb development, *erg* is also expressed in the anterior and posterior necrotic zones (Margarida Santos thesis) and the same expression pattern is observed in duck embryos (Figure 8A, black arrowheads). These findings point to a conserved role of *erg* during the apoptotic process. Throughout the whole period studied, *erg* expression showed a direct relationship with the distribution of the programmed cell death areas in different species, in particular with INZ.

In addition to its expression in the apoptotic areas, *erg* expression was also detected in the dermomyotome (shown in Margarida Santos thesis). Furthermore *erg* transcripts appeared at the hindlimb medial part, corresponding to the myogenic condensations present at the limb (Figure 6 A-C), in myogenic cells of the differentiating muscles (Figure 6, E and K) and surrounding the dorsal and ventral tendons (Figure 6L).

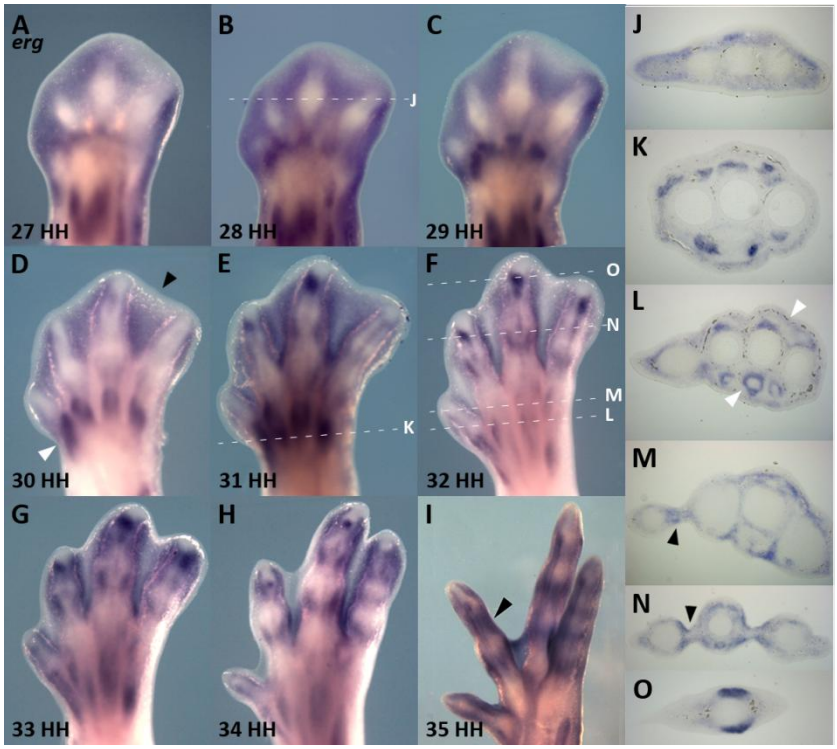

Figure 6 – *erg* expression during digit development. *In situ* hybridization for *erg* in developing autopods at stages 27HH (A), 28HH (B), 29 HH (C), 30HH (D), 31HH (E), 32HH (F), 33HH (G), 34HH (H) and 34HH (I). J, K and L-O are transverse sections of B, E and F, respectively. *In situ* hybridization for *erg* shows that it is expressed in the interdigital areas prior the physiological cell death initiation (A-C and J). At stage 30, *erg* is still expressed at the entire interdigital space (D, black arrowhead), but as development proceeds and ICD begins, *erg* expression becomes progressively restricted to the side of the digits (E-I and N, black arrowhead). At stage 35 *erg* is expressed surrounding the phalanxes and the remaining interdigit (I). Throughout digit development, *erg* is also present in muscular masses (A-H, D and L, white arrowheads) and around the tendons (L).

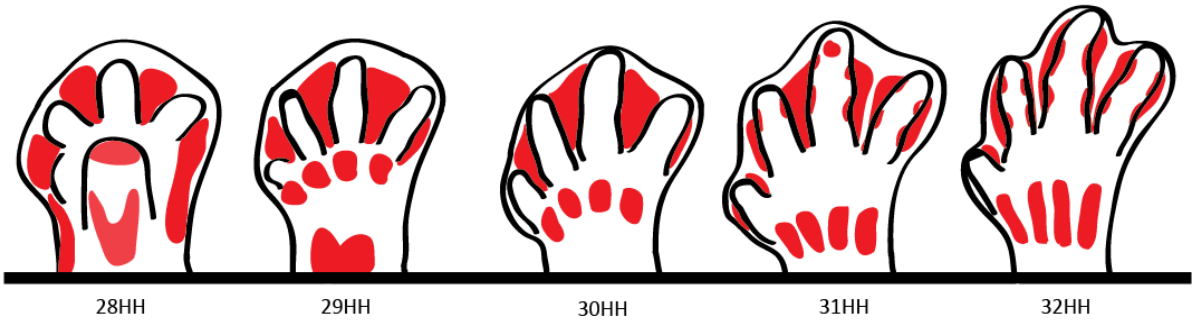

Figure 7 –Schematic representation of *erg* expression pattern during digit development. *erg* begins to be expressed throughout the interdigital areas (28HH) and in the myogenic cells. As ICD initiates, *erg* transcripts become progressively restricted to digit sides and to the differentiating muscles.

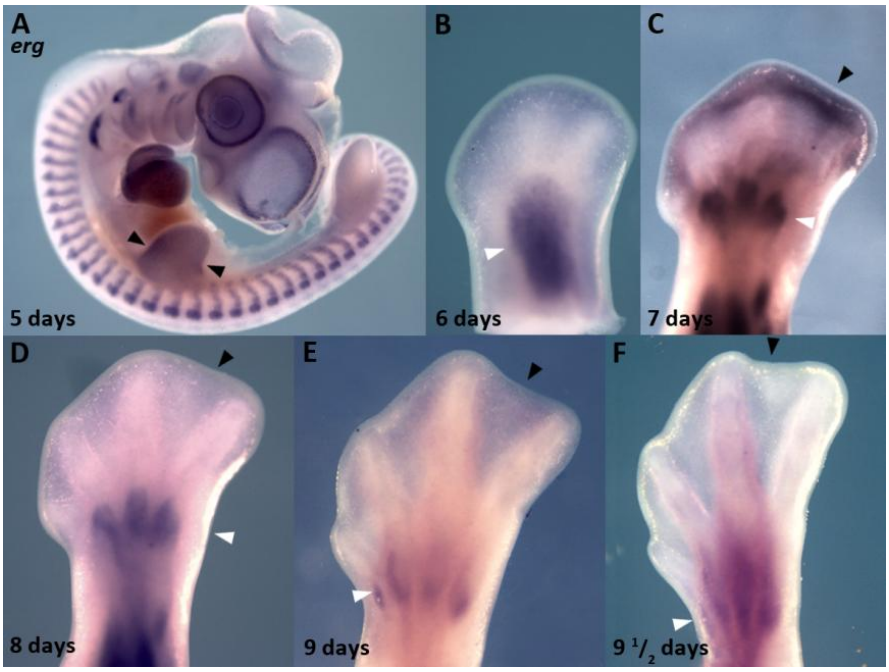

Figure 8 – *erg* expression pattern in duck. *In situ* hybridization for *erg* in duck embryos shows that during limb development this gene is expressed at the anterior and posterior necrotic zones (A, arrowheads). As shown in chick limbs, *erg* is expressed in myogenic masses (B-F white arrowheads). Between 7-8 days of incubation, *erg* is expressed at the distal tip of the interdigit (C, black arrowhead) where cell death will occur. Note that the interdigital domains of erg become restricted distally coincidently with the zones of interdigital cell death in the duck. At later stages (E-F) *erg* interdigital expression is lost (black arrowheads) but remains expressed in the muscle masses (white arrowheads).

Inhibition of *erg* activity during digit development

Since chick and duck *erg* expression patterns suggest that this gene would be a good candidate to be involved in interdigital cell death (ICD) control, we performed loss-of-function studies to further understand its possible role in the apoptotic process. To approach that, we used chick embryos between stage 28HH and 29HH and implanted beads soaked in 10mM ERG Inhibitor (M5060 E-4031 Sigma), a specific ERG activity blocker, to functionally challenge the intercellular dynamics of potassium. In order to continuously deliver the drug, several beads were implanted in the same interdigital space at different time points. The first bead was implanted into the third interdigit of the right hindlimb, and 6 to 7 hours later a second bead substituted or was implanted distally to the first one when cell death has not yet started in the interdigits. A third bead was implanted 12h later and when embryos reached stage 30-31HH they were processed for cell death analysis by acridine orange vital staining (Figure 9). There was a visible reduction of cell death in the INZ after ERG inhibitor-soaked beads implantation (Figure 9A) when compared with the control interdigit (Figure 9A') and PBS bead treated limbs (Figure 9B). Note the inhibition of cell death in the area close to the ERG inhibitor bead (Figure 9A). The interdigit apoptotic pattern was not altered after a PBS-bead implantation (Figure 9B) when compared to the control leg (Figure 9B'). Interdigital longitudinal sections of treated limbs were also analyzed for apoptotic DNA fragmentation by TUNEL assay, together with the immunolabeling for phospho-histone H3 (Figure 11). As showed for the acridine orange staining, interdigital apoptosis was reduced, but apoptosis at joint formation was still visible

after ERG bead implantation (Figure 11A, red arrowhead). Cell proliferation assessed by immunolabeling of phospho-histone H3 did not differ from non-treated limbs.

To check if ERG inhibitor blockage could be enough to affect normal interdigit regression, we fixed embryos 3 to 4 days after the first bead implanted. Limbs were also stained with Alcian green to ensure that the drug delivery did not affect normal limb chondrogenesis (Figure 10). As predicted, upon ERG treatment limbs present syndactyly (Figure 10A). Chondrogenesis was not affected by the bead implantation treatment (Figure 10a' and Figure 10A).

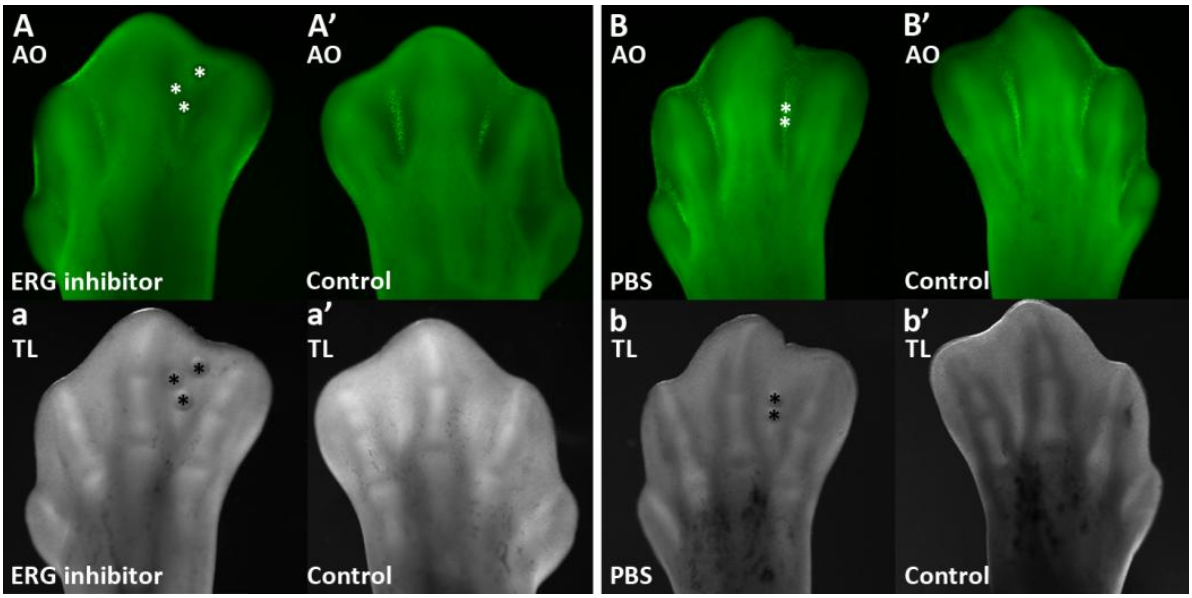

Figure 9 – Acridine orange (AO) cell death analysis after inhibition of ERG activity. (A) After ERG inhibitor-soaked beads implantation into the interdigit mesenchyme there is a visible reduction of cell death in the INZ, when compared to their counterlateral control ones (A') and PBS-soaked bead treated limbs (B). Cell death pattern remains the same after PBS-beads implantation (B) when compared with control leg (B'). The panels below (a-b') illustrate the limb morphology in transmitted light (TL) to ensure that there are no changes in differentiation of the phalanxes. Asterisks (*) refer to bead location.

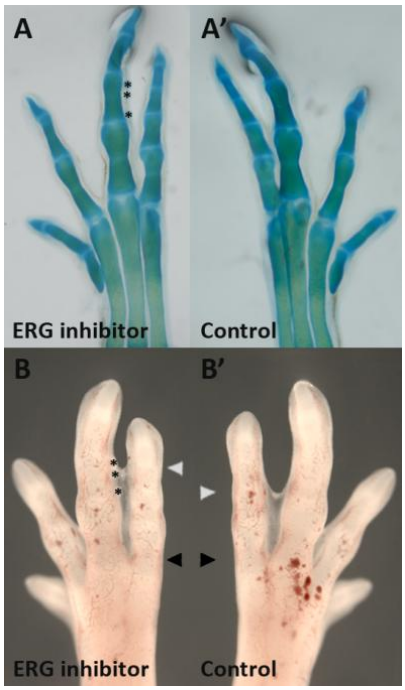

Figure 10 – Morphological analysis after ERG inhibitor bead implantation. A' and B' are control limbs of A and B, respectively. (A) Alcian green staining of experimental limb after ERG inhibitor-soaked beads implantation illustrating that no changes in chondrogenesis are detected after treatment. Plates B and B' show the interdigital physical differences between ERG inhibitor treated limbs (B) and corresponding control leg (B'), 3 days after bead implantation. Black and white arrowheads point out the interdigital proximal and distal limits, respectively. Asterisks (*) refer to bead location.

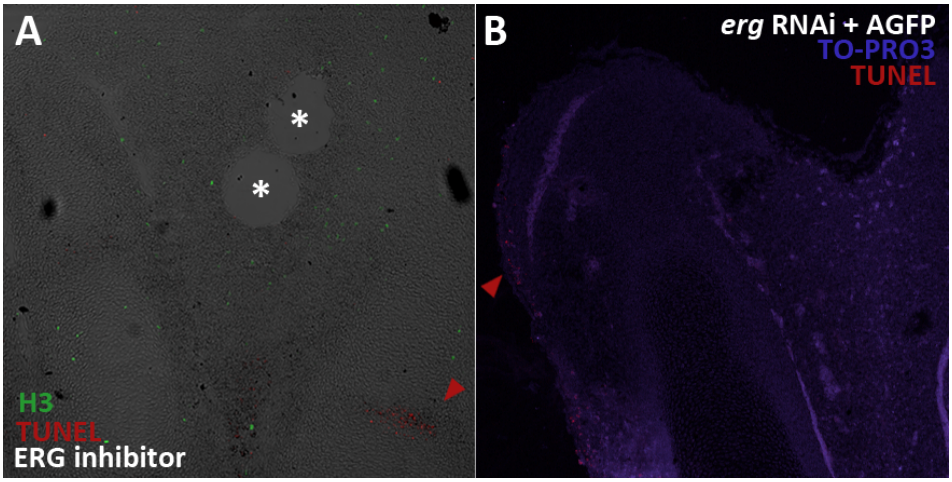

Figure 11 – TUNEL apoptotic cell labeling of experimental interdigits after *erg* inhibition. (A) Longitudinal section of the third interdigital area with TUNEL staining of apoptotic programmed cell death (red) combined with phospho-histone H3 labeling of proliferating cells (green), 36h after ERG inhibitor-soaked beads implantation. Asterisks (*) refer to bead location. (B) Longitudinal section of the third interdigital area after pSUPER-*erg* RNAi and pCAGGS-AGFOP co-electroporation showing the apoptotic programmed cell death pattern by TUNEL staining (red) and TO-PRO3 nuclei labeling (blue). Red arrowheads indicates the locals of TUNEL apoptotic cells.

Since blocking *erg* activity inhibited interdigital cell death (ICD), we proceeded to study the expression pattern of genes known to be involved in the ICD process, namely *fgf8* (Hernandez-Martinez *et al*, 2009), *fgf10*, *msx2* (end effector of BMP-mediated apoptosis (Marazzi et al., 1997)), *bambi* (as a *bmp4* readout), *snail* (Montero et al., 2001) and *smad8* (Figure 12). After ERG inhibitor treatment *erg* expression pattern was not altered (n=8, Figure 12A) meaning that its activity does not influence *erg* normal mRNA transcription. *In situ* hybridization for the pseudoreceptor *bambi* (BMP and activin membrane-bound inhibitor) (n=3, Figure 12B) shows a slight inhibition surrounding the beads implanted. On the other hand, loss of ERG potassium channel activity resulted in strong downregulation of *smad8* (n=13, Figure 12C), *snail* (n=7, Figure 12D) and *fgf10* (n=1, Figure 12E) expression 36h after ERG inhibitor treatment. Note *fgf10* inhibition at the distal interdigit and digits tips. Conversely, *fgf8* expression at the AER was upregulated upon ERG inhibitor treatment (n=3, Figure 12F, arrowhead) when compared with the control limb (Figure 12F'). *In situ* hybridization for *msx2* showed that its expression was unaltered 7h after treatment with ERG inhibitor (n=3, Figure 12G). However, 36h after bead implantation there was a slight inhibition of *msx2* expression around the beads (n=8, Figure 12H) and by hour 60, *msx2* downregulation was clearly observable (n=1, Figure 12I).

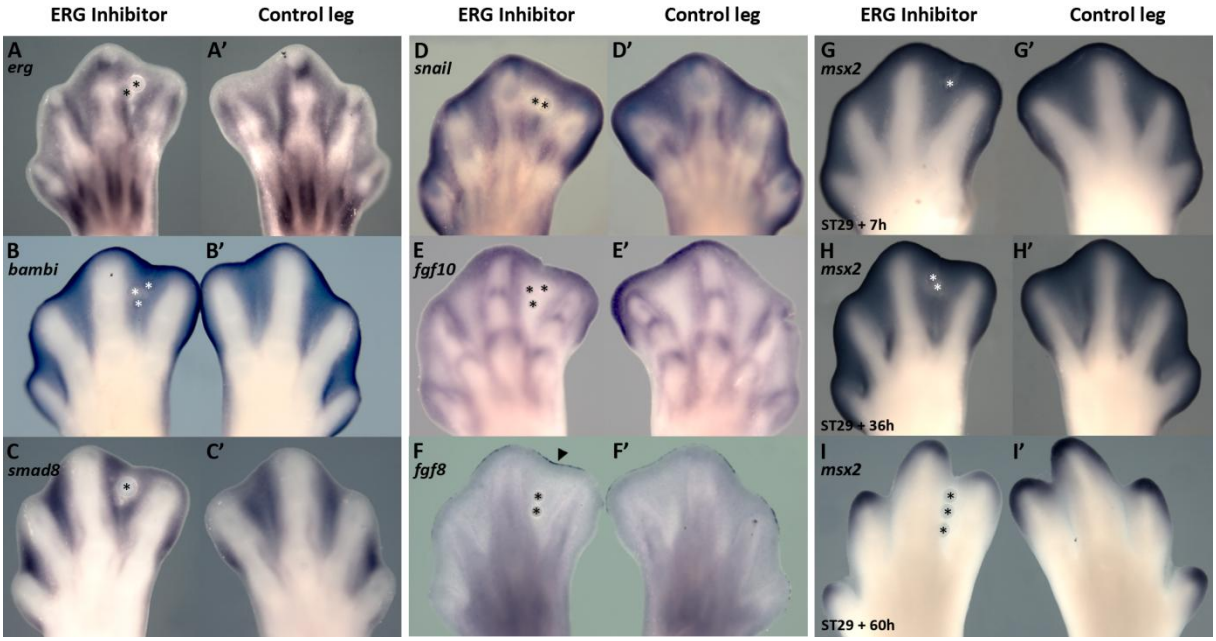

Figure 12 – Regulation of genes involved in chick interdigital cell death following ERG inhibitor treatment. A'-I' are control limbs of A-I, respectively. Upon ERG inhibitor bead implantation *erg* expression pattern is unaltered (A). *In situ* hybridization for *bambi* (B) shows a slight inhibition around the beads (*) implanted. *smad8* (C), *snail* (D) and *fgf10* (E) expression patterns are strongly downregulated 36h after ERG inhibitor treatment. Note *fgf10* inhibition at the digits tips. *fgf8* (F) expression is upregulated upon ERG inhibitor treatment (see arrowhead) when compared with the control limb (F'). *In situ* hybridization for *msx2* (G-I) shows that its expression is unaltered 7h after treatment with ERG inhibitor (G). However, 36h after ERG inhibitor-soaked bead implantation (H) there is a slight inhibition of *msx2* expression around the beads. This *msx2* downregulation is clearly observable 60h after ERG inhibitor treatment (I). Asterisks (*) refer to bead location.

Electroporation was also used as an alternative loss-of-function assay. We used the pSUPER vector to drive the synthesis of RNAi transcripts that suppress endogenous RNA activity leading to a loss-of-function phenotype (Figure 4). Silencing of *erg* was achieved by co-electroporation of both pCAGGS-AGFP and a pSUPER- *erg* RNAi, while control of the procedure was done by electroporation of pCAGGS-AGFP alone. Silencing of ERG potassium signaling through *erg* RNAi electroporation promoted the persistence of the interdigital membrane of the electroporated interdigit, resembling a syndactyly phenotype (Figure 14C). Electroporation of pCAGGS-AGFP alone (Figure 14D) did not affect interdigital membrane regression. There was a significant difference between experimental (pSUPER- *erg* RNAi + pCAGGS-AGFP co-electroporated, n=75, Figure 14C) and respective control limb (non-electroporated, Figure 14C'), while pCAGGS-AGFP electroporated interdigit (n=38, Figure 14D) and corresponding control leg (Figure 14D') showed the same regression pattern. RNAi experimental interdigits were significant longer (Figure 14A) and with a greater area (Figure 14B) than the control ones. Both experimental and control electroporated limbs did not show differences in chondrogenesis.

As expected, after suppression of *erg* endogenous RNA activity there was *erg* mRNA downregulation (Figure 13A). We then studied the effect of *erg* silencing through specific RNAi electroporation in the expression of genes known to be involved in the apoptotic process.

In contrast to the ERG inhibitor treatment results, *smad8* (Figure 13B), *fgf10* (Figure 13C), *fgf8* (Figure 13D), *msx2* (Figure 13E, F) and *bambi* (Figure 13I, J) expression patterns were not altered after *erg* silencing, compared with the corresponding control legs. *In situ* hybridization for *snail* showed an mRNA reduction on the electroporated area (Figure 13G) including the third interdigit and the neighboring digits close to their epiphysis. Silencing of *erg* 48h after electroporation resulted in a slight inhibition of *snail* expression at the distal end of the interdigit, near the digits (Figure 13H).

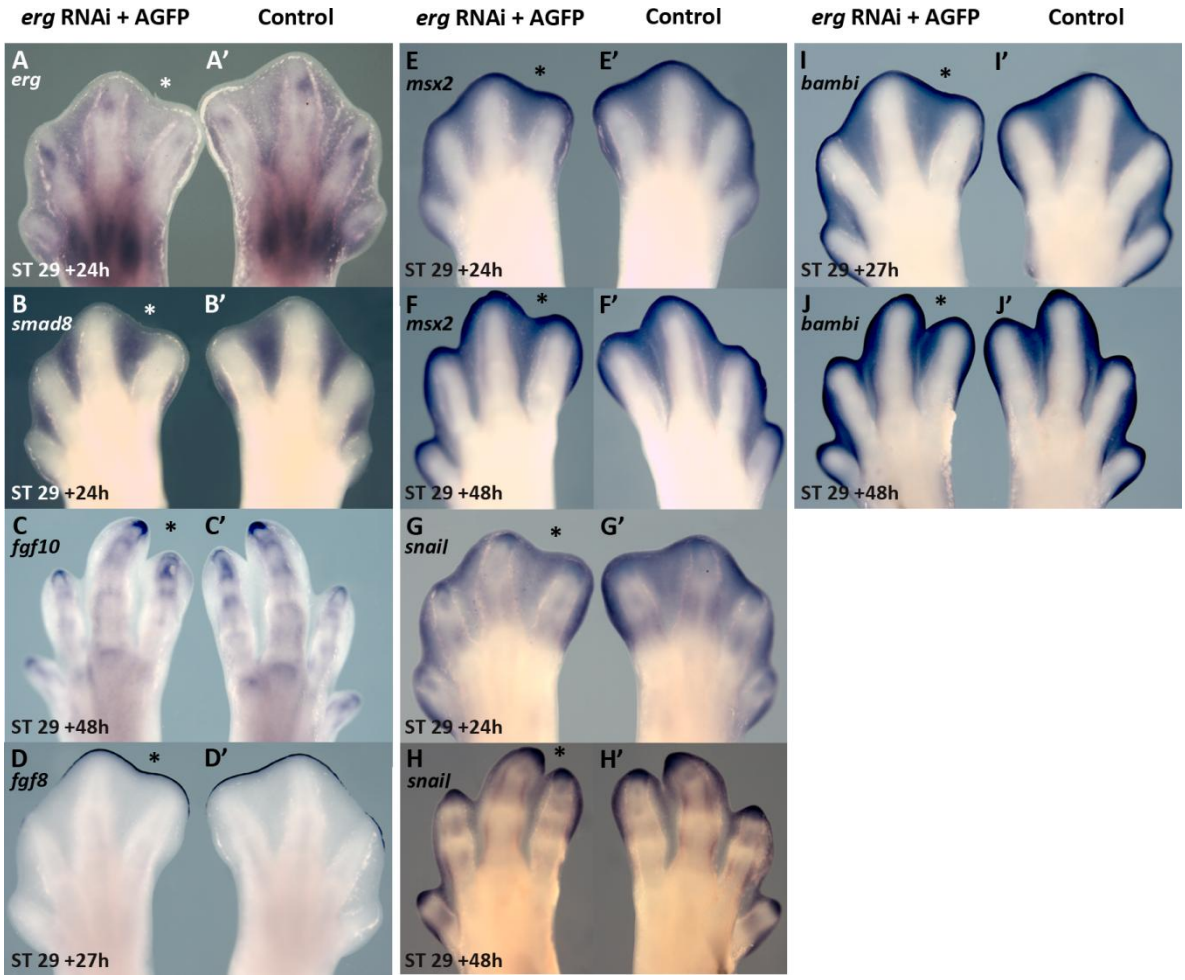

Figure 13 – *erg* RNAi electroporation effects on genes involved in the apoptotic/programmed cell death process. A'-J' are control limbs of A-I, respectively. Whole-mount *in situ* hybridization for *erg* after *erg* RNAi electroporation in the third interdigital area of chick right hindlimbs confirms its mRNA dowregulation (A). *smad8* (B), *fgf10* (C), *fgf8* (D), *msx2* (E, F) and *bambi* (I, J) expression pattern is unaltered after co-electroporation of *erg* RNAi with AGFP, comparing with respective control legs. *In situ* hybridization for *snail* shows an inhibition on the electroporated area (*) including third interdigit and neighboring digits (near the ephisis), 24h after *erg* RNAi electroporation (G). 48h after *erg* electroporation *snail* expression is only slightly inhibited at the distal end of the interdigit, near the digits (H). Asterisks (*) refer to the electroporated interdigital area of the experimental limb.

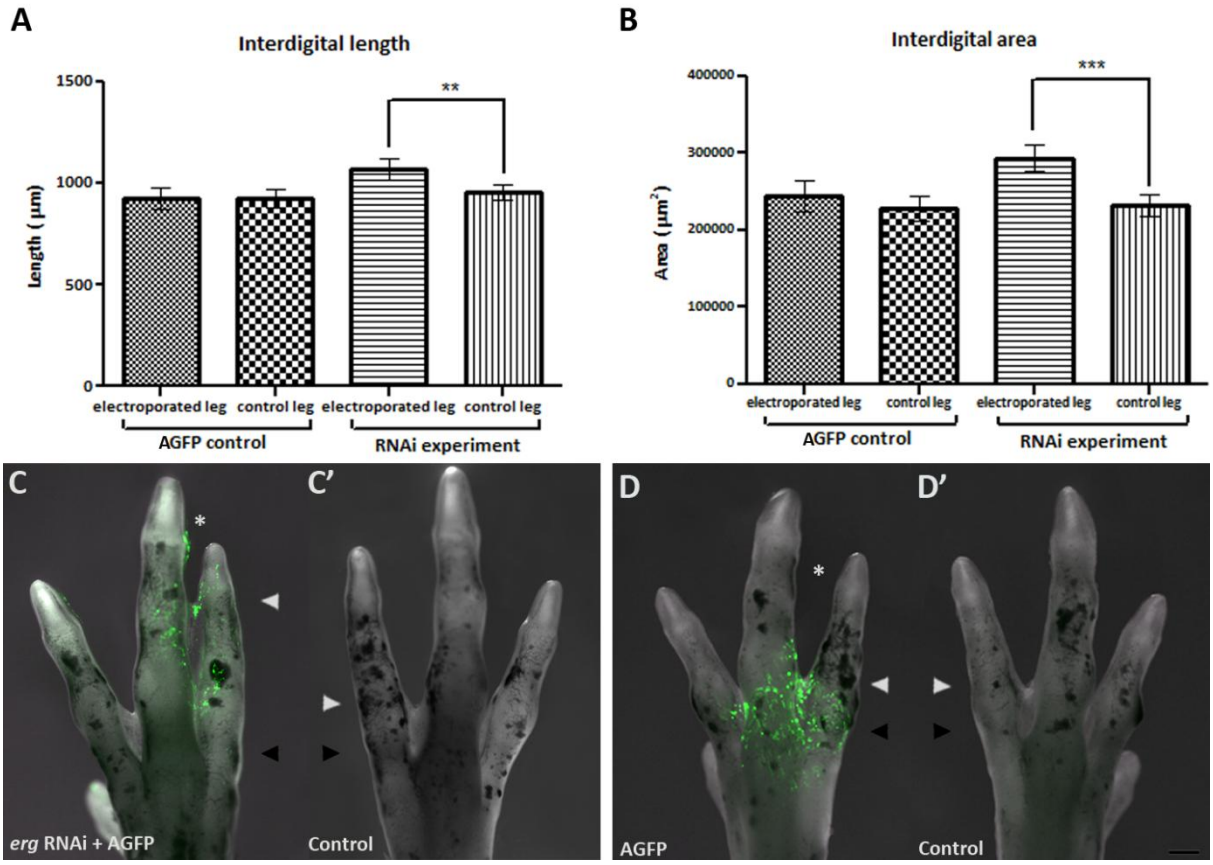

Figure 14 – Loss-of-function studies through *erg* RNAi electroporation. Electroporation was done at the third interdigit area of stage 28-29 HH chick right hindlimbs. Plates A and B illustrate the interdigital physical differences between *erg* RNAi + AGFP co-electroporation and AGFP electroporated controls 4 days after the procedure. (A) Interdigits co-electroporated with *erg* RNAi + AGFP show a significant length increase when compared to their counterlateral control ones (left hindlimb, not electroporated) $^{**}p < 0.01$, whereas AGFP electroporated controls do not show any difference. Such increase is even more striking as an area increase, $^{***}p < 0.0001$ (B). (C) Silencing of *erg* through co-electroporation of *erg* RNAi and AGFP (shown in green) at stage 28-29HH chick hindlimbs results in a syndactyly phenotype at the third interdigital level, 4 days after the procedure. Black arrowheads indicate the proximal limit of the interdigit and white arrowheads its distal limit to show that this structure is extended distally after *erg* loss-of-function (compare C with C'). AGFP electroporated controls (D) do not show any difference when compared to the non-electroporated leg (D'). C, C', D and D' asterisks (*) refer to the electroporated interdigital area of the experimental limb. Black and white arrowheads point out the interdigital proximal and distal limits, respectively. Bar in C-D', 500µm.

Interdigital longitudinal sections of electroporated treated limbs were also analyzed for apoptotic DNA fragmentation by the terminal deoxynucleotidyl transferase-mediated dUTP-TRIC nick end labeling (TUNEL) assay, together with the immunolabeling of phospho-histone H3 proliferanting cells. We observed reduction of apoptosis after *erg* RNAi electroporation (Figure 11B). Cell proliferation asessed by immunolabeling of phospho-histone H3 did not differ from non-treated limbs (data not shown).

Regulation of *erg* expression through FGF signaling

Signaling by BMPs (Macias et al., 1997), FGFs (Montero et al., 2001) and retinoic acid (Rodriguez-Leon et al., 1999) have been shown to have an effect in interdigital cell death control in chicken limb buds. To understand the relationship between these signaling pathways and erg, we compared the expression of *erg* upon local delivery of those molecules into the distal mesenchyme of the hindlimb interdigit.

When ICD begins, *fgf8* expression in the AER overlying the interdigital cell death is downregulated (Ganan et al., 1998). In one hand, this *fgf8* inhibition has been demonstrated to be one of the crucial steps for triggering of interdigital apoptosis (Hernandez-Martinez et al., 2009). But, on the other hand, blocking of FGF signaling inhibits BMP apoptotic induction as its local application inhibits cell death (Montero et al., 2001).

The possible influence of the FGF signaling pathway on *erg* expression was analyzed by local application of FGF8, FGF10 and SU5402 (a specific FGF-inhibitor) soaked beads. FGF8-soaked beads implantation resulted in *erg* downregulation 10h (n=6, Figure 15A) and 20h (n=6, Figure 15B) after treatment. Interdigital downregulation of *erg* in chicken hindlimbs was also observed 20h (n=3, Figure 15C) and 24h (n=4, Figure 15D) after local implantation of beads carrying FGF10. To further analyze this relationship we performed the complement experiment, inhibiting specific FGF-signaling through SU5402-soaked bead implantation (n=12, Figure 15E) what did not affect *erg* expression (n=12, Figure 15E). PBS-soaked beads were employed as a control for the bead implantation procedure and didn't alter *erg* expression (n=6, Figure 15F).

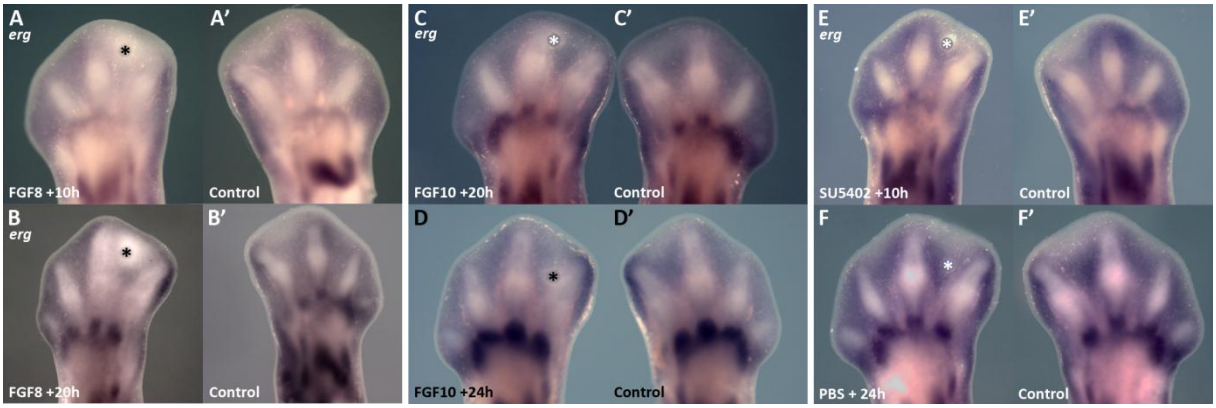

Figure 15 – Regulation of interdigital expression of *erg* in chick hindlimbs through FGF signaling. Panels A and B illustrate the downregulation of interdigital *erg* expression in chicken limbs 10h (A) and 20h (B) after FGF8 bead implantation (asterisks). Panels A' and B' are the respective control legs. Plates C and D show the interdigital downregulation of *erg* in chicken hindlimbs 20h (C) and 24h (D) after local delivery of FGF10 soaked beads, and C' and D' are the corresponding controls. Conversely, local application of FGF-specific inhibitor, SU5402, does not affect *erg* expression (E). PBS-soaked beads were employed as a control for the bead implantation procedure and do not alter *erg* expression (F). In all experiments right hindlimbs were manipulated and left hindlimbs were employed as a control. Asterisks (*) refer to the local of bead implantation.

RA signaling regulates *erg* expression

Retinoic acid (RA) local application in the interdigital spaces of the chick limb bud accelerates interdigital programmed cell death through the induction of BMP signaling cascade (Dupe et al., 1999; Rodriguez-Leon et al., 1999). It is still unclear if RA regulates apoptosis in the INZ only by inducing BMP signaling, but there are evidences that RA counteracts AER-FGF8 survival signaling through *Bax* induction (Hernandez-Martinez et al., 2009). To understand if RA mechanisms of action could influence *erg* activity, we performed implantations of beads soaked in RA and its inhibitor Citral

Interdigital *erg* expression is downregulated 15h after RA local bead implantation (Figure 16A) when compared with the control limb (Figure 16A'). This downregulation is enhanced when two RA-beads are implanted together (Figure 16B) suggesting that *erg* inhibition is dose dependent. This may be due to an increase in cell death induction by RA (mediated by the BMP transduction pathway) and therefore the dying cells stop expressing the gene, or a direct reduction in *erg* expression. Blockage of RA signaling through Citral-soaked bead implantion (Figure 16C) and control (Figure 16C') did not seem to exert an influence in *erg* expression 20h after treatment.

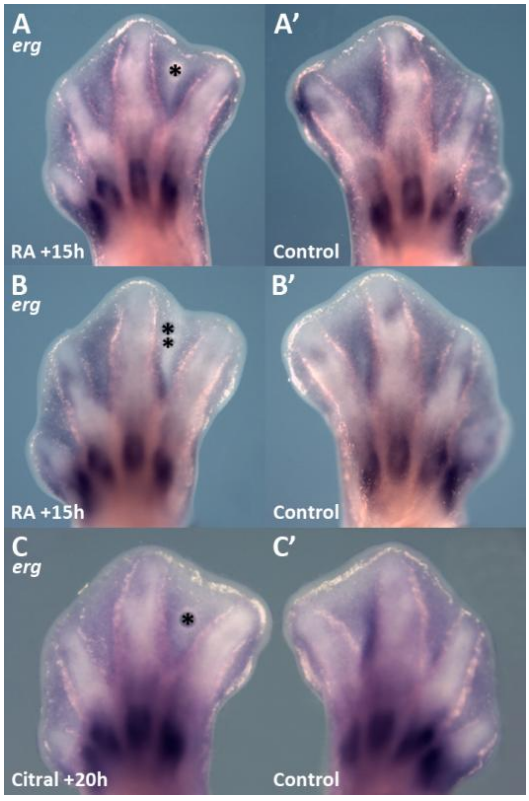

Figure 16 – Retinoic acid (RA) signaling modulates *erg* expression in the interdigital area of chick hindlimbs. *In situ* hybridization for *erg* demonstrated the downregulation of the gene expression in chick hindlimbs 15h after RA local delivery (A) compared with the control limb (A'). *erg* expression is strongly reduced when two RA-beads are implanted together (B). RA signaling inhibition through Citral-soaked bead implantion (C) does not seem to exert an influence in *erg* expression 20h after treatment, when compared to the control leg (C'). Asterisks (*) refer to bead location.

Regulation of *erg* expression by BMP signaling

It has been shown that the family of Bone Morphogenetic Proteins (BMPs) plays a major role during limb interdigital apoptosis, promoting cell death in the INZ (Macias et al., 1997; Montero and Hurle, 2010; Zuzarte-Luis et al., 2004). To assess the relationship of BMP activity in the expression of *erg*, we analyzed the effects of local application of BMPs (BMP2 and BMP4) and their antagonists (Noggin and Gremlin) into the undifferentiated mesenchyme of the chick developing limb.

In situ hybridization for *erg* showed that 3h after BMP2 implantation there was a slight proximal upregulation of *erg* expression near the digits (n=21, Figure 17A). Conversely, 6h after BMP2 implantation (Figure 17B) there was a reduction of *erg* transcripts. Moreover, BMP4 downregulated *erg* 3h (Figure 17C) and 6h (Figure 17D) after bead implantation. Local implantation of the BMP antagonists Gremlin (Figure 17E) and Noggin (Figure 17F) did not show a significant change in *erg* expression 20h and 24h after treatment, respectively. This suggests that the BMP transduction pathway could act synergistically with other pathways that may also induce and maintain *erg* expression.

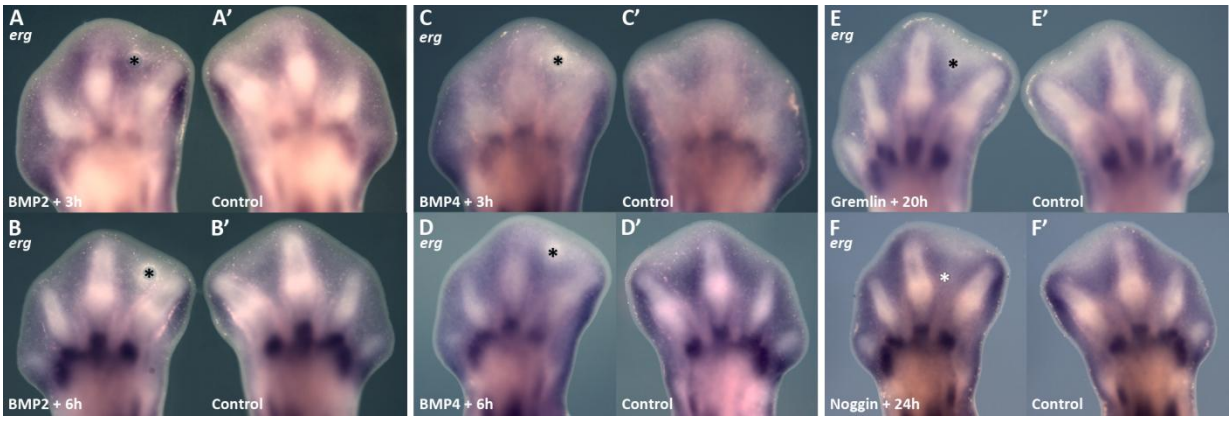

Figure 17 – Regulation studies of interdigital *erg* expression in chick limbs by BMP signaling. A'-F' are control limbs of A-F, respectively. (A) 3h after BMP2-soaked bead implantation there is a slight proximal upregulation of *erg* expression, near the digits (as at 2h after bead implantation, data not shown). Conversely, 6h after BMP2 bead implantation (B) there is an inhibition of *erg* expression. On the other hand, BMP4 downregulated *erg* 3h (C) and 6h (D) after bead implantation. Local implantation of BMPs' antagonists Gremlin (E) and Noggin (F) do not show a significant change in *erg* expression 20h and 24h after treatment, respectively. Asterisks (*) refer to bead location.

IV. Discussion

Interdigital programmed cell death establishment in the developing limb autopod is accompanied by the occurrence of corresponding domains of *erg* expression. This study analyzes whether these coincident events are functionally correlated.

erg expression co-localizes with apoptotic zones

At stage 26 HH *erg* is expressed in the area corresponding to the anterior and posterior necrotic zones (ANZ and PNZ), as well as in the central mesenchyme (Margarida Santos thesis). This expression pattern is also found in the duck at corresponding stages (Figure 8A). When digits appear, *erg* expression is detected in the whole interdigits prior to the onset of programmed cell death and is maintained throughout this process in the chicken embryo (Figure 6 and 7). In duck *erg* is also expressed at the INZ but its pattern of expression becomes restricted to the most distal part of the interdigit, the apoptotic areas in this specie (Figure 8C, black arrowhead) (Hurle and Colvee, 1982). These findings are consistent with a conserved role for *erg* controlling apoptosis during digit development.

However, *erg* expression is not detected at the areas of cell death present in the developing interphalangeal joints nor in the opaque patch. These findings point to differences in the death machinery among different areas of limb cell death as proposed by Zuzarte-Luis and colleagues (Zuzarte-Luis et al., 2007).

Transcripts for *erg* can be found also in the migrating myogenic precursors (Margarida Santos thesis) from the somites. This suggests that ERG would be important for cell migration. One of the first features that precede apoptosis is cell detachment, the same mechanism that occurs during migration (Hurle and Fernandez-Teran, 1983; Martin-Bermudo et al., 1998; Montero et al., 2001). Therefore, the expression domain of *erg* in the INZ could indicate that this gene would be responsible for the initial steps of programmed cell death that involve loss of contact between cells.

erg gene triggers apoptosis

ERG activity could cause important homeostatic modifications able to influence the functional properties of the enzymatic cascades implicated in the cell death mechanisms. According to these findings we expected that *erg* loss-of-function experiments would cause inhibition of interdigital cell death promoting syndactyly phenotypes. A syndactyly phenotype is characterized by the absence of free digits and is accompanied by the persistence of an interdigital membrane (Montero and Hurlé, 2010). After *erg* activity downregulation or mRNA silencing a significant increase in the interdigital membrane length is observed and the resulting syndactyly is due to the lack of apoptosis (Figure 10B

and 14C, respectively). This phenotype is similar to that obtain after inhibition of BMP, RA or FGF signaling (Ganan et al., 1996; Merino et al., 1999b; Montero et al., 2001; Rodriguez-Leon et al., 1999).

In fact, *erg* loss of function is followed by downregulation of different genes involved in programmed cell death, namely *msx2* (Chen and Zhao, 1998; Marazzi et al., 1997), *smad8* (Zuzarte-Luis and Hurle, 2005), *bambi*, *fgf10* and *snail* (Montero et al., 2001) (Figure 12). Downregulation of these genes suggests that ERG activity is involved in the BMP signaling, one of the major contributors to cell death in the INZ (Ganan et al., 1996; Zuzarte-Luis et al., 2004). Also, *erg* seems to controls the level of FGF signaling in the interdigital space, what is crucial to trigger apoptosis (Montero et al., 2001). Moreover, *erg* must be involved in the regulation of detachment of cells due to the lack of *snail* after its inhibition (Montero et al., 2001). This is in accordance with the expression pattern of *erg*, detected when myogenic precursors are migrating into the limb buds (Christ and Brand-Saberi, 2002).

Besides this, ERG influence is also observed at the ectodermal level. *Fgf8* downregulation is needed for the normal onset of cell death as it regulates death RA levels by both decreasing the expression of its synthesizer *raldh2* and increasing RA degradation through *cyp26b1* (Hernandez-Martinez et al., 2009). We have observed that *fgf8* expression is enhanced and maintained after ERG blockage (Figure 12F). These results confirm that *fgf8* downregulation is essential to trigger apoptosis and it is controlled by the activity of the interdigital mesenchyme through ERG action. This action could be mediated by BMP signaling that is activated or maintained by ERG function. In the future, analysis of BMP activity through immunostainings for the phosphorylated forms of SMAD8 would be needed to confirm or discard this hypothesis. Besides these activities, it has been shown that ectodermal Wnt/β-catenin signaling can positively regulate *fgf8* possibly antagonizing the epithelial derived BMP transduction pathway. The balance of Wnt/β-catenin signal in the limb ectoderm including the AER can regulate interdigital apoptosis (Villacorte et al., 2010). A negative regulation of Wnt/β-catenin through *erg* transduction pathway is a good alternative to the activation of ectodermal BMPs. This does not have to be mutually exclusive; ERG could, at the same time, decrease Wnt/β-catenin expression and activate ectodermal BMPs.

The differences observed after bead treatment or electroporation in the expression of these genes could be due to a stronger and wider inhibition of ERG activity by the chemical antagonist. Electroporation is not able to target all the cells at the interdigital level and inhibition of cell death is less effective.

erg expression is regulated by apoptotic signals

We have tested how different apoptotic inducers control *erg* expression. One major contributor to cell death is RA signaling (Rodriguez-Leon et al., 1999). We have found that after RA treatment *erg* expression is inhibited and, moreover, this inhibition is dose dependent (Figure 16A and B, respectively). But inhibition of RA signaling cannot downregulate *erg* expression (Figure 16C). Cell

death induced by RA is mediated by BMP activation (Rodriguez Leon et al., 1999). In our work, BMP treatment enhances *erg* expression at initial stages of induced apoptosis and then *erg* transcripts are no longer detected when cell death is massive (Figure 17A and B respectively). This is in accordance with the expression pattern observed for *erg* during limb development (Figure 6). At initial stages, *erg* expression is activated and then, when cell death occurs in the whole interdigit *erg* expression is downregulated. This inhibition may be due to BMP accelerated cell death induction observed at the interdigits (Ganan et al., 1996), which downregulates several genes (Zuzarte-Luis et al., 2004), *erg* included. Also, using BMP antagonists, *erg* expression is not downregulated (Figure 17 E and F). This suggests that BMPs are not the only inducers of *erg* activity. Another molecules involved in apoptotic induction are FGFs (Montero et al., 2001). Local treatments with FGFs inhibit *erg* expression what can have a double interpretation (Figure 15). Initially, FGFs promote survival and this can lead to *erg* downregulation to prevent its action on cell detachment. After that, FGFs induce massive cell death and, at that point, *erg* expression is no longer detected, something that also occurs physiologically and after BMP treatment (reviewed in Zuzarte-Luis and Hurle, 2004). When FGF signaling is inhibited, *erg* expression is unaltered (Figure 15E). Therefore, inhibition of RA, BMP or FGF signaling by itself is not sufficient to inhibit *erg* expression what suggests that there must be a cooperative activity among these molecules and/or others to induce and maintain *erg* transcription. Experiments combining the inhibition of these signaling pathways would be needed to clarify which are the key contributors to this regulation.

ERG potassium channel involvement in cell detachment

Ion flows are important for a broad range of cell functions, of which excitability is only a small part. Rational modulation of ion currents and ion channel expression may therefore be potential control mechanisms for a variety of cell behaviors (Sundelacruz et al., 2009). Ion microenvironment together with extracellular matrix may control these cell behaviors.

Our evidences point to *erg* as modulator of the cell detachment needed for both migration and apoptosis. In fact, recent molecular data implicated KCNQ1 potassium channels and NaV sodium channels in the regulation of migration and invasiveness of several stem-like cell types. These findings enhance the idea that stem cells can migrate in physiological-strength electric gradients (Morokuma et al., 2008).

In cancer, the expression of different ion channels regulates specific progression of the neoplastic phenotype ranges. ERG channels have been detected in many primary human cancers and exert pleiotropic effects in cancer cells. It is though that *erg* signaling modulates adhesive interactions with the extracellular matrix. The activity of ERG, seems to be mediated by formation of macromolecular complexes with membrane receptors, especially integrins. In fact, β1 integrin subunit can activate hERG1 and, conversely, once ERG is activated by integrins, can modulate signaling pathways downstream to integrin receptors. (Cherubini et al., 2005; Pillozzi and Arcangeli, 2010).

In our model, ERG could be contributing to integrin signaling. Integrins are expressed during limb development (Bajanca and Thorsteinsdottir, 2002) but further expression analysis has to be done during digit development to clarify this point.

Moreover, it has been shown that Snail regulates apoptosis in cooperation with the FGF and BMP signaling (Montero et al., 2001). It is likely that cell death induction through *snail* activity is due to its powerful activity in decreasing cell adhesion by the repression of the expression of cadherins (Cano et al., 2000). Physiological expression of *snail* is strongly inhibited in the area of ERG activity blockage (Figure 12D) what implies that *erg* exert a crucial role in *snail* activity that could be also mediated through integrin signaling.

Proposed model for *erg* activity

Our results support a model in which *erg* activation precedes the onset of cell death. The action of this molecule would be the activation of cell detachment needed for physiological cell death. Also, *erg* activity would be responsible for the inhibition of FGF signaling from the overlying ectoderm, crucial to activate apoptosis, by enhancing BMP activity. Conversely, BMP and BMP RA-induced signaling can induce and maintain *erg* expression but in a redundant fashion since inhibition of one of this pathways is not sufficient to downregulate *erg* expression. In the final period of apoptosis, ERG activity is not longer needed and its expression is abolished by accumulation of BMP signaling (Figure 18).

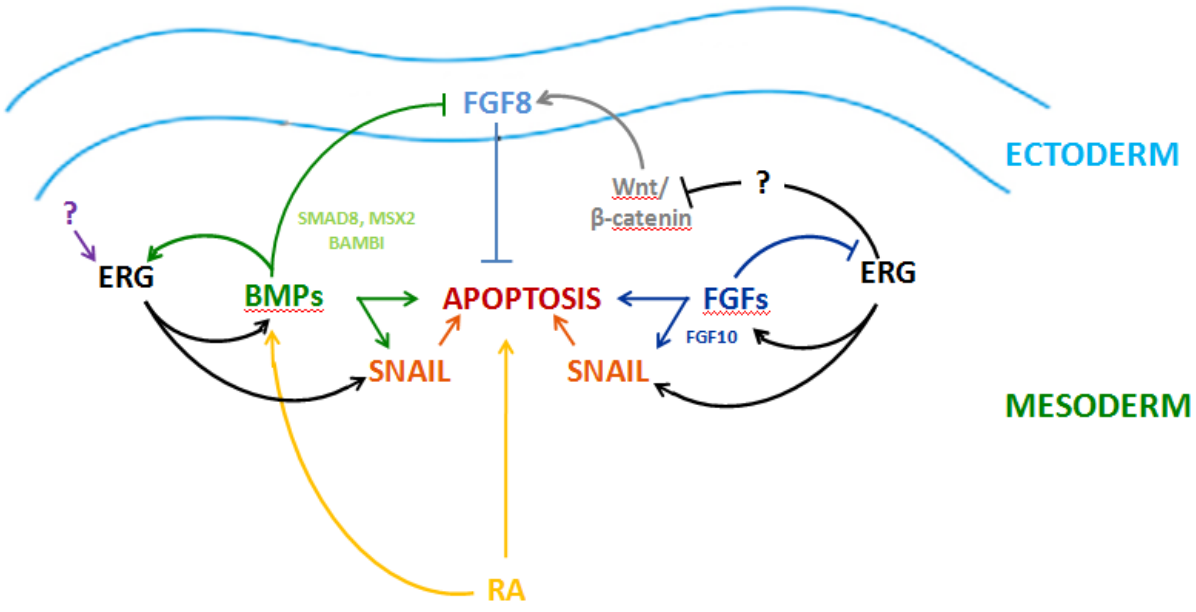

Figure 18 – Proposed model for *erg* activity. ERG activates cell detachment through upregulation of *snail*, which in turns induce apoptosis. *Erg* also upregulates FGFs at mesenchymal level (FGF10), which are known to induce apoptosis. Interdigital cell death is also initiated by *fgf8* dowregulation, possibly by *erg* activation of ectodermal BMPs. Note that *erg* negative regulation of *wnt/β-catenin* is only illustrated as an alternative idea. Moreover, expression of *erg* is upregulated by BMPs, but un alternative transduction pathway seems to be also involved in this activation.

Concluding remarks

One set of experiments that need to be done in the future to clarify *erg* induction and maintenance is the inhibition, at the same time, of FGF, RA and BMP signaling. This way, we could depict the regulation of *erg* expression and understand which of these molecules are working in a combined manner.

Also, interdigital electroporation should be improved to target more mesenchymal cells and western blots could be done to assess protein downregulation after RNAi treatment. At the same time, it would be interesting to clone full length *erg* to overexpress it in the whole footplate and confirm if, only by itself, is able to induce or accelerate programmed cell death.

V. References

Abrams, J. M., White, K., Fessler, L. I. and Steller, H. (1993). Programmed cell death during Drosophila embryogenesis. Development 117, 29-43.

Altizer, A. M., Moriarty, L. J., Bell, S. M., Schreiner, C. M., Scott, W. J. and Borgens, R. B. (2001). Endogenous electric current is associated with normal development of the vertebrate limb. Dev Dyn 221, 391-401.

Bajanca, F. and Thorsteinsdottir, S. (2002). Integrin expression patterns during early limb muscle development in the mouse. Mech Dev 119 Suppl 1, S131-4.

Burg, E. D., Remillard, C. V. and Yuan, J. X. (2006). K+ channels in apoptosis. J Membr Biol 209, 3-20.

Cano, A., Perez-Moreno, M. A., Rodrigo, I., Locascio, A., Blanco, M. J., del Barrio, M. G., Portillo, F. and Nieto, M. A. (2000). The transcription factor snail controls epithelial-mesenchymal transitions by repressing E-cadherin expression. *Nat Cell Biol* 2, 76-83.

Capdevila, J., Tsukui, T., Rodriquez Esteban, C., Zappavigna, V. and Izpisua Belmonte, J. C. (1999). Control of vertebrate limb outgrowth by the proximal factor Meis2 and distal antagonism of BMPs by Gremlin. Mol Cell 4, 839-49.

Chautan, M., Chazal, G., Cecconi, F., Gruss, P. and Golstein, P. (1999). Interdigital cell death can occur through a necrotic and caspase-independent pathway. Curr Biol 9, 967-70.

Chen, Y. and Zhao, X. (1998). Shaping limbs by apoptosis. J Exp Zool 282, 691-702.

Cherubini, A., Hofmann, G., Pillozzi, S., Guasti, L., Crociani, O., Cilia, E., Di Stefano, P., Degani, S., Balzi, M., Olivotto, M. et al. (2005). Human ether-a-go-go-related gene 1 channels are physically linked to beta1 integrins and modulate adhesion-dependent signaling. Mol Biol Cell 16, 2972-83.

Christ, B. and Brand-Saberi, B. (2002). Limb muscle development. Int J Dev Biol 46, 905-14.

Dealy, C. N., Roth, A., Ferrari, D., Brown, A. M. and Kosher, R. A. (1993). Wnt-5a and Wnt-7a are expressed in the developing chick limb bud in a manner suggesting roles in pattern formation along the proximodistal and dorsoventral axes. Mech Dev 43, 175-86.

Dupe, V., Ghyselinck, N. B., Thomazy, V., Nagy, L., Davies, P. J., Chambon, P. and Mark, M. (1999). Essential roles of retinoic acid signaling in interdigital apoptosis and control of BMP-7 expression in mouse autopods. Dev Biol 208, 30-43.

Fallon, J. F. and Cameron, J. (1977). Interdigital cell death during limb development of the turtle and lizard with an interpretation of evolutionary significance. J Embryol Exp Morphol 40, 285-9.

Felipe, A., Vicente, R., Villalonga, N., Roura-Ferrer, M., Martinez-Marmol, R., Sole, L., Ferreres, J. C. and Condom, E. (2006). Potassium channels: new targets in cancer therapy. Cancer Detect Prev 30, 375-85.

Fernandez-Teran, M. A., Hinchliffe, J. R. and Ros, M. A. (2006). Birth and death of cells in limb development: a mapping study. Dev Dyn 235, 2521-37.

Francis-West, P. H., Parish, J., Lee, K. and Archer, C. W. (1999). BMP/GDF-signalling interactions during synovial joint development. Cell Tissue Res 296, 111-9.

Ganan, Y., Macias, D., Basco, R. D., Merino, R. and Hurle, J. M. (1998). Morphological diversity of the avian foot is related with the pattern of msx gene expression in the developing autopod. Dev Biol 196, 33-41.

Ganan, Y., Macias, D., Ros, M. A., Merino, R. and Hurle, J. M. (1996). Control of skeletogenesis and programmed cell death in the developing avian limb bud by growth factors. Int J Dev Biol Suppl 1, 189S.

Gilbert, Scott F. (2006) Developmental Biology, Eighth Edition

Greenwood, I. A., Yeung, S. Y., Tribe, R. M. and Ohya, S. (2009). Loss of functional K+ channels encoded by ether-a-go-go-related genes in mouse myometrium prior to labour onset. J Physiol 587, 2313-26.

Hamburger, V. and Hamilton, H.L. (1992). A series of normal stages in the development of the chick embryo, (reprinted from journal of morphology, vol 88, 1951). Developmental Dynamics 195: 231-272

Hernandez-Martinez, R., Castro-Obregon, S. and Covarrubias, L. (2009). Progressive interdigital cell death: regulation by the antagonistic interaction between fibroblast growth factor 8 and retinoic acid. Development 136, 3669-78.

Huang, C. and Hales, B. F. (2002). Role of caspases in murine limb bud cell death induced by 4-hydroperoxycyclophosphamide, an activated analog of cyclophosphamide. Teratology 66, 288-99.

Hurle, J. M. and Colvee, E. (1982). Surface changes in the embryonic interdigital epithelium during the formation of the free digits: a comparative study in the chick and duck foot. J Embryol Exp Morphol 69, 251-63.

Hurle, J. M. and Fernandez-Teran, M. A. (1983). Fine structure of the regressing interdigital membranes during the formation of the digits of the chick embryo leg bud. J Embryol Exp Morphol 78, 195-209.

Hurle, J. M., Ros, M. A., Climent, V. and Garcia-Martinez, V. (1996). Morphology and significance of programmed cell death in the developing limb bud of the vertebrate embryo. Microsc Res Tech 34, 236-46.

Kawakami, Y., Capdevila, J., Buscher, D., Itoh, T., Rodriguez Esteban, C. and Izpisua Belmonte, J. C. (2001). WNT signals control FGF-dependent limb initiation and AER induction in the chick embryo. Cell 104, 891-900.

Khokha, M. K., Hsu, D., Brunet, L. J., Dionne, M. S. and Harland, R. M. (2003). Gremlin is the BMP antagonist required for maintenance of Shh and Fgf signals during limb patterning. Nat Genet 34, 303-7.

Macias, D., Ganan, Y., Sampath, T. K., Piedra, M. E., Ros, M. A. and Hurle, J. M. (1997). Role of BMP-2 and OP-1 (BMP-7) in programmed cell death and skeletogenesis during chick limb development. Development 124, 1109-17.

Marazzi, G., Wang, Y. and Sassoon, D. (1997). Msx2 is a transcriptional regulator in the BMP4-mediated programmed cell death pathway. Dev Biol 186, 127-38.

Martin-Bermudo, M. D., Dunin-Borkowski, O. M. and Brown, N. H. (1998). Modulation of integrin activity is vital for morphogenesis. J Cell Biol 141, 1073-81.

Mercader, N., Leonardo, E., Piedra, M. E., Martinez, A. C., Ros, M. A. and Torres, M. (2000). Opposing RA and FGF signals control proximodistal vertebrate limb development through regulation of Meis genes. Development 127, 3961-70.

Merino, R., Ganan, Y., Macias, D., Economides, A. N., Sampath, K. T. and Hurle, J. M. (1998). Morphogenesis of digits in the avian limb is controlled by FGFs, TGFbetas, and noggin through BMP signaling. Dev Biol 200, 35-45.

Merino, R., Macias, D., Ganan, Y., Economides, A. N., Wang, X., Wu, Q., Stahl, N., Sampath, K. T., Varona, P. and Hurle, J. M. (1999a). Expression and function of Gdf-5 during digit skeletogenesis in the embryonic chick leg bud. Dev Biol 206, 33-45.

Merino, R., Rodriguez-Leon, J., Macias, D., Ganan, Y., Economides, A. N. and Hurle, J. M. (1999b). The BMP antagonist Gremlin regulates outgrowth, chondrogenesis and programmed cell death in the developing limb. Development 126, 5515-22.

Montero, J. A., Ganan, Y., Macias, D., Rodriguez-Leon, J., Sanz-Ezquerro, J. J., Merino, R., Chimal-Monroy, J., Nieto, M. A. and Hurle, J. M. (2001). Role of FGFs in the control of programmed cell death during limb development. Development 128, 2075-84.

Montero, J. A. and Hurle, J. M. (2010). Sculpturing digit shape by cell death. Apoptosis 15, 365-75.

Morokuma, J., Blackiston, D., Adams, D. S., Seebohm, G., Trimmer, B. and Levin, M. (2008). Modulation of potassium channel function confers a hyperproliferative invasive phenotype on embryonic stem cells. Proc Natl Acad Sci U S A 105, 16608-13.

Odani, N., Ito, K. and Nakamura, H. (2008). Electroporation as an efficient method of gene transfer. Dev Growth Differ 50, 443-8.

Pautou, M. P. (1974). Comparative development of interdigital morphogenetic necrosis in the foot of chick and duck embryos. C R Acad Sci Hebd Seances Acad Sci D 278, 2209-12.

Parr, B. A., Shea, M. J., Vassileva, G. and McMahon, A. P. (1993). Mouse WNT genes exhibit discrete domains of expression in the early embryonic CNS and limb buds. Development 119, 247-261.

Pillozzi, S. and Arcangeli, A. (2010) Physical and Functional Interaction between Integrins and hERG1 Channels in Cancer Cells; Integrins and Ion Channels: Molecular Complexes and Signaling; *Chapter Category: Channels and Transporters*

Rodriguez-Leon, J., Merino, R., Macias, D., Ganan, Y., Santesteban, E. and Hurle, J. M. (1999). Retinoic acid regulates programmed cell death through BMP signalling. Nat Cell Biol 1, 125-6.

Salas-Vidal, E., Valencia, C. and Covarrubias, L. (2001). Differential tissue growth and patterns of cell death in mouse limb autopod morphogenesis. Dev Dyn 220, 295-306.

Sauka-Spengler, T. and Barembaum, M. (2008). Gain- and loss-of-function approaches in the chick embryo. Methods Cell Biol 87, 237-56.

Saunders, J. W. (1948) The proximo-distal sequence of origin of limb parts of the chick wing and the role of the ectoderm. *J. Exp. Zool.* 108, 363–404.

Saunders, J. W., Jr. and Gasseling, M. T. (1962). Cellular death in morphogenesis of the avian wing. Dev Biol 5, 147-78.

Saunders, J. W., Jr. (1966). Death in embryonic systems. *Science* 154, 604-12.

Scholz, E. P., Niemer, N., Hassel, D., Zitron, E., Burgers, H. F., Bloehs, R., Seyler, C., Scherer, D., Thomas, D., Kathofer, S. et al. (2009). Biophysical properties of zebrafish ether-a-go-go related gene potassium channels. Biochem Biophys Res Commun 381, 159-64.

Sundelacruz, S., Levin, M. and Kaplan, D. L. (2009). Role of membrane potential in the regulation of cell proliferation and differentiation. Stem Cell Rev 5, 231-46.

Tabin, C. and Wolpert, L. (2007). Rethinking the proximodistal axis of the vertebrate limb in the molecular era. Genes Dev 21, 1433-42.

Veeck, J. and Dahl, E. (2010). RNA expression analysis on formalin-fixed paraffin-embedded tissues in TMA format by RNA in situ hybridization. Methods Mol Biol 664, 135-50.

Villacorte, M., Suzuki, K., Hayashi, K., de Sousa Lopes, S. C., Haraguchi, R., Taketo, M. M., Nakagata, N. and Yamada, G. (2010). Antagonistic crosstalk of Wnt/beta-catenin/Bmp signaling within the Apical Ectodermal Ridge (AER) regulates interdigit formation. Biochem Biophys Res Commun 391, 1653-7.

Zeller, R. (2010). The temporal dynamics of vertebrate limb development, teratogenesis and evolution. Curr Opin Genet Dev 20, 384-90.

Zeller, R., Lopez-Rios, J. and Zuniga, A. (2009). Vertebrate limb bud development: moving towards integrative analysis of organogenesis. Nat Rev Genet 10, 845-58.

Zuzarte-Luis, V. and Hurle, J. M. (2002). Programmed cell death in the developing limb. Int J Dev Biol 46, 871-6.

Zuzarte-Luis, V. and Hurle, J. M. (2005). Programmed cell death in the embryonic vertebrate limb. Semin Cell Dev Biol 16, 261-9.

Zuzarte-Luis, V., Montero, J. A., Kawakami, Y., Izpisua-Belmonte, J. C. and Hurle, J. M. (2007). Lysosomal cathepsins in embryonic programmed cell death. Dev Biol 301, 205-17.

Zuzarte-Luis, V., Montero, J. A., Rodriguez-Leon, J., Merino, R., Rodriguez-Rey, J. C. and Hurle, J. M. (2004). A new role for BMP5 during limb development acting through the synergic activation of Smad and MAPK pathways. Dev Biol 272, 39-52.

Appendix I – Buffers, Solutions and Media

Reagents:

Probe Transcription	**Source**	**Reference**
T3 RNA polymerase	Promega	P208C
T7 RNA polymerase	Promega	P207B
Tampão de transcrição 5X	Promega	P118B
SP6 RNA polymerase	Promega	P108B
DIG RNA Labeling Mix	Roche	11277073910
RNAsin	Promega	N2111
***in situ* hybridization**		
Sheep Serum	Chemicon	S22-100ML
Anti-Digoxigenin-AP, Fab fragmentos	Roche	11 093 274 910
BM Purple	Roche	11442074001
Blocking Reagent	Roche	11096176001
Immunohistochemistry		
Goat Serum	Sigma-Aldrich	G9023
DAPI	Invitrogen	D1306
TO-PRO 3 (1mM)	Invitrogen	T3605
Tissue Tek O.C.TTM Compound	Sakura Finetek	4583
VECTASHIELD® HardSet™ Mounting medium	Vector Laboratories	H-1400
Dulbecco's Modified Eagle's Medium	Sigma	D-9161

Solutions and Buffers:

PBS	
NaCl	137 mM
KCl	2.7 mM
Na_2HPO_4	10 mM
KH_2PO_4	2 mM
	Adjust to pH 7,4 with HCl

PBT	
PBS	1x
Tween-20	0,1% (v/v)

PFA	
PFA	4%
	in PBS

1X TAE

EDTA	2mM
Acetic acid	20mM
Tris-acetate (pH 8,0)	40mM

Ethidium bromide Solution

Et_2Br	10 mg/mL
	Made in milliQ H_2O

Sodium Acetate

CH3COONa	3M
	Adjust to pH 5,3

Lithium Chloride

LiCl	4M

6% hydrogen peroxide

H_2O_2	6% (v/v)
	in PBT

Glycine Solution

Glycine	2mg/mL
	in PBT

Hybridization solution

Formamide	50% (v/v)
SSC (pH 7,5)	5x
Tween-20	0.2% (v/v)
tRNA	50µg/ml
heparin	50µg/ml
	made in milliQ H_2O

Solution I

Formamide	50% (v/v)
20x SSC (pH 4,5)	20% (v/v)
Tween-20	2% (v/v)
	made in milliQ H_2O

Solution III

Formamide	50% (v/v)
20x SSC (pH 4,5)	10% (v/v)
	made in milliQ H_2O

MABT

Maleic acid	100mM
NaCl	150mM
Tween-20	0,1% (v/v)
	Adjust to pH 7,5 with NaOH 1N

Blocking Solution

Fetal Calf Serum heat inactivated	10% (v/v)
Blocking Reagent	2% (w/v)
	in MABT

Antibody Solution

Blocking Solution	
Anti-Digoxigenin-AP, Fab fragments	1:2000

MABT with levamisol

Levamisol	0,0048% (w/v)
	in MABT

NTMT

Tris-HCl (pH 9,5)	100mM
$MgCl_2$	50mM
NaCl	100mM
Tween-20	0,10%
	made in milliQ H_2O

PBS-Sucrose Solution

Sucrose	10% (w/v)
	in PBS

Gelatin

Gelatin	10% (w/v)
	in PBS-Sucrose solution

TBS

NaCl	140 mM
KCl	2.7 mM
Tris HCl (pH 8,0)	25 mM

Blocking Solution

Triton-X	0,5% (v/v)
Sheep Serum	3% (v/v)
	in TBS

TBS ++

Triton-X	0,1% (v/v)
Sheep Serum	3% (v/v)
	in TBS

TdT Buffer (pH 7,75)

Tris-HCl	1.182g
	in milliQ H_2O, adjust to pH 7,2
Sodium Cacodylate	7.49g
Cobalt (II) Chloride Anhydrous	0.032g
	adjust to pH 7,75

SSC + EDTA

EDTA	0.9306g
NaCl	8.7575g
Sodium Citrate	4.4118g
	in 500ml of milliQ H_2O

Acid Alcohol

	70%
Ethanol	(v/v)
HCL 1N	1% (v/v)

Alcian Green

Alcian Green (Sigma)	0,1% (w/v)
	made in acid alcohol

Appendix II – Plasmid Maps

Restriction map of pCR®II-TOPO® Vector:

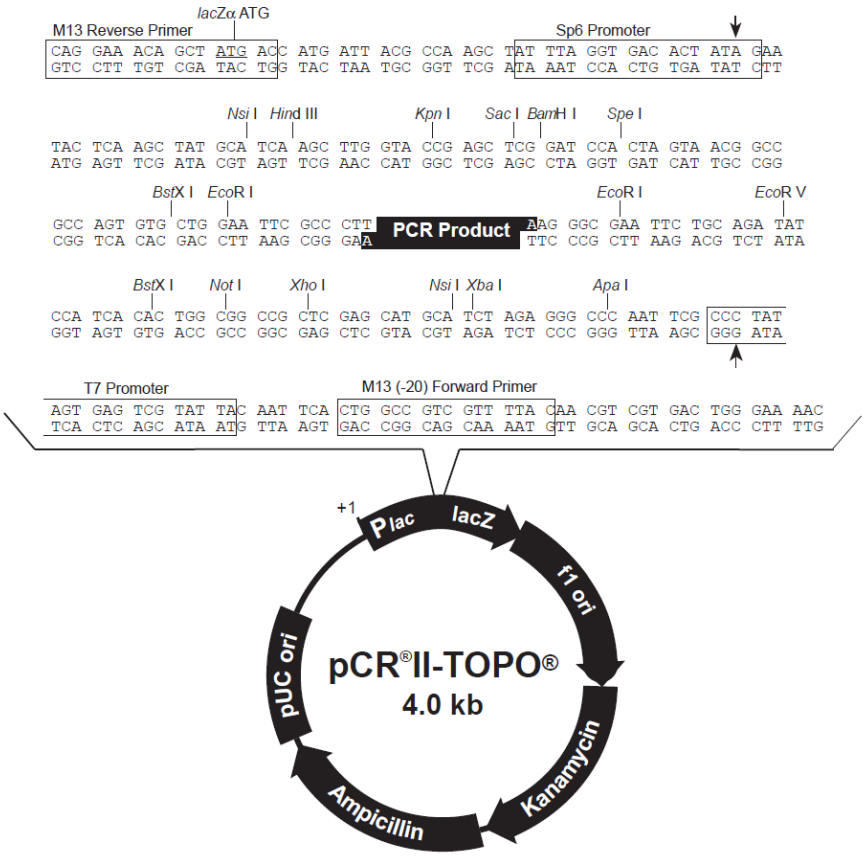

Sequence of the multiple cloning site is annotated (TOPO TA Cloning Kit, Invitrogen).

Restriction map of pBluescript II SK Vector:

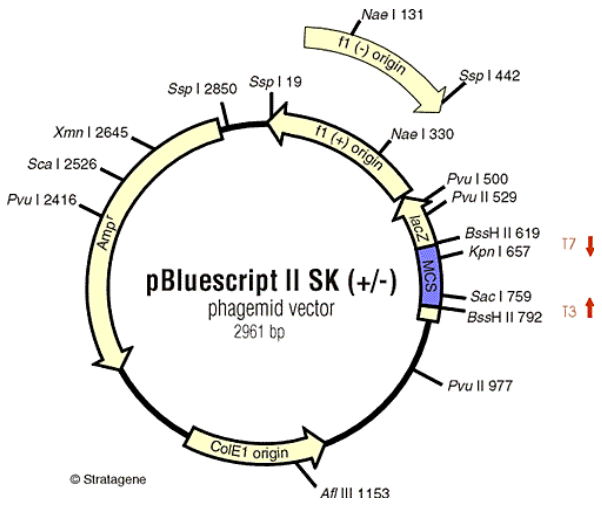

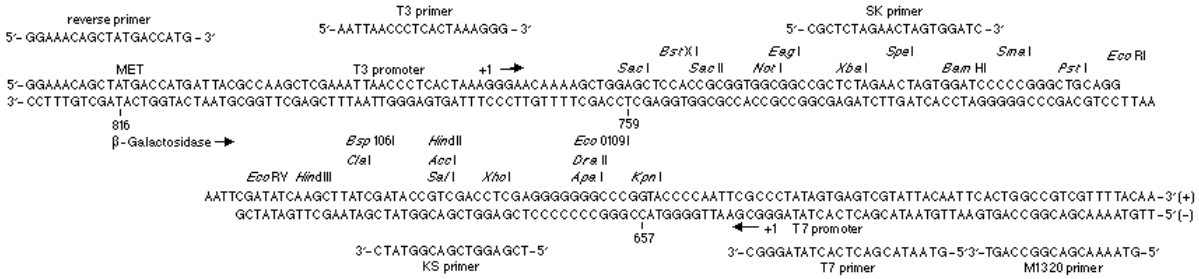

In the vector diagram some restriction sites are annotated with their respective location in the sequence. MSC (in blue) – Multiple cloning site. Sequence of multiple cloning site is bellow the diagram (Stratagene).

Restriction map of pGEM Vector :

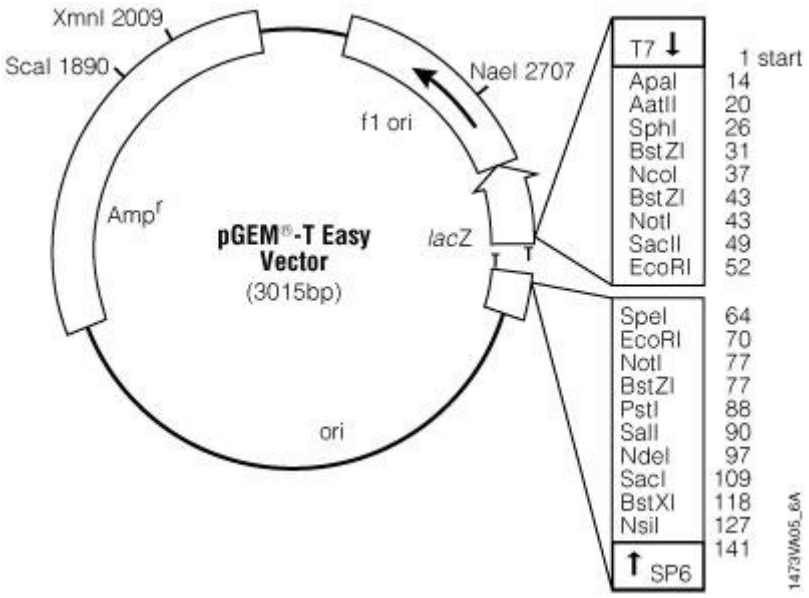

Restriction map of pSUPER Vector :

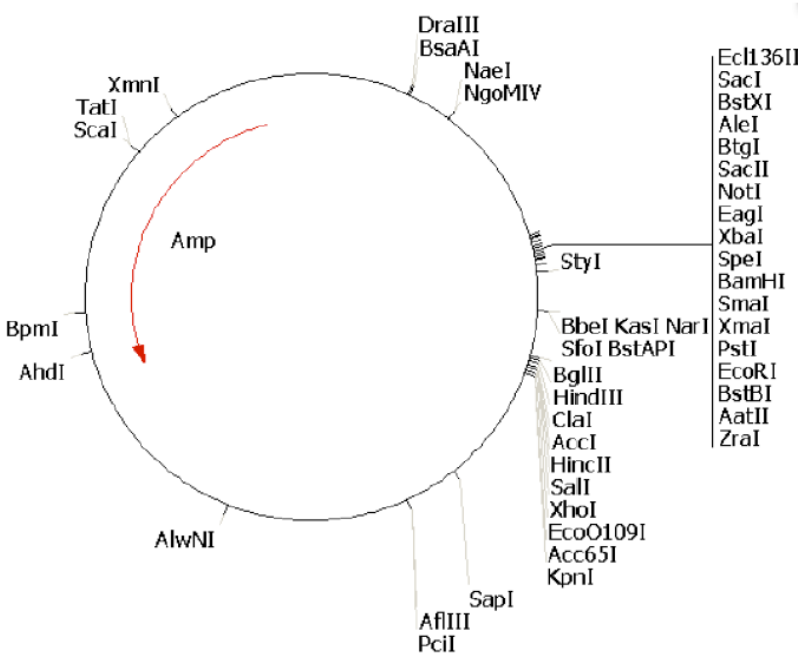

Restriction map of pGAGGS-AGFP Vector :

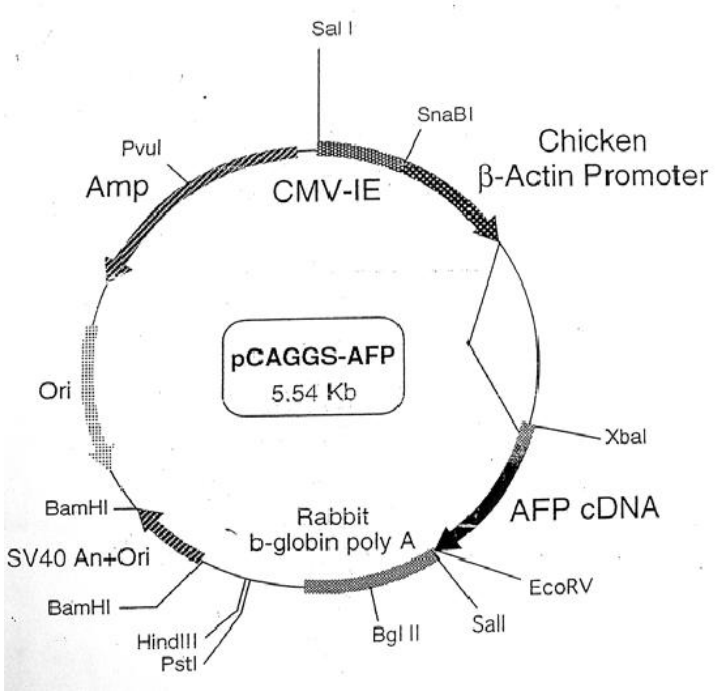

Appendix III – *erg*'s alignment

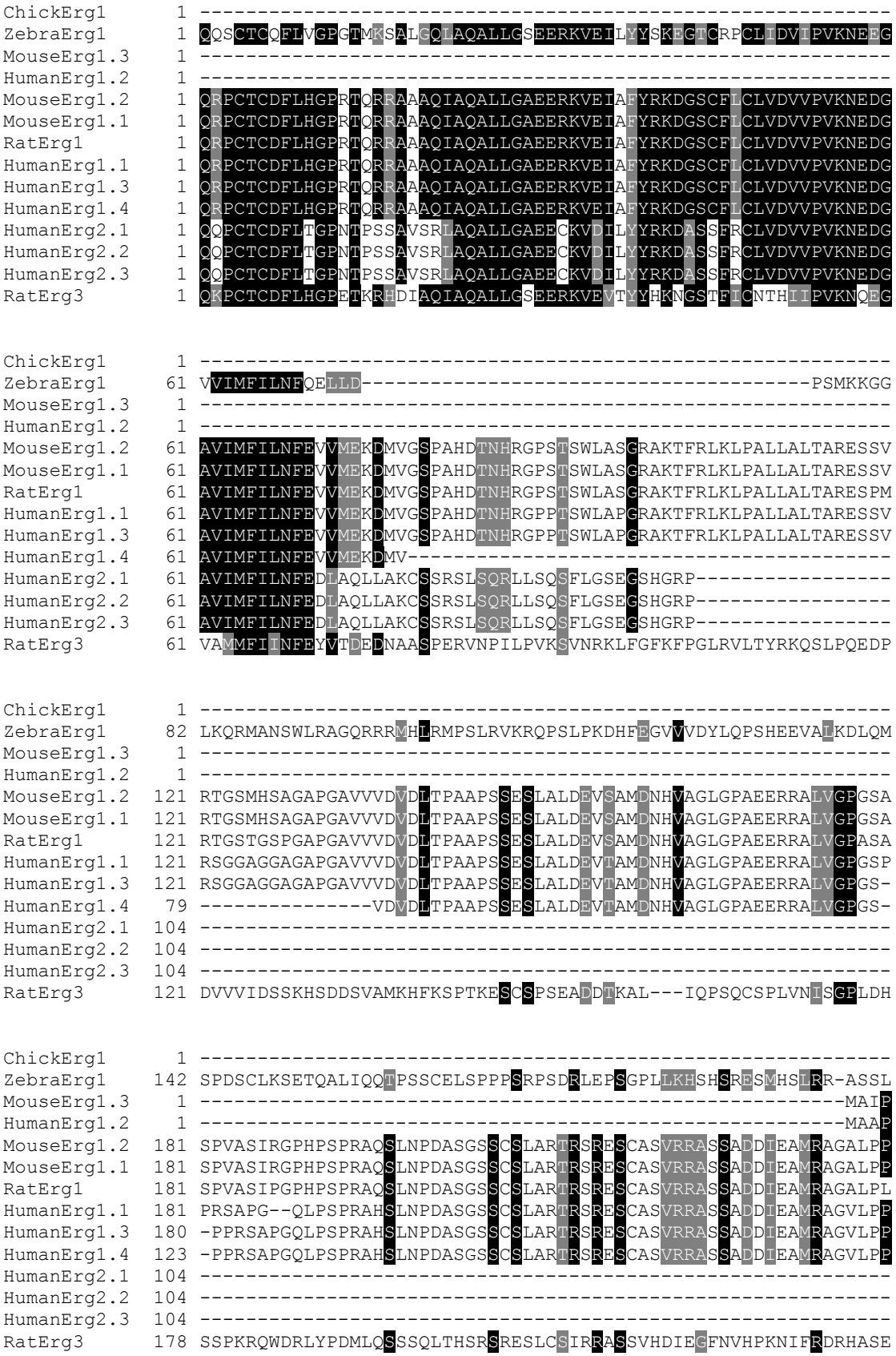

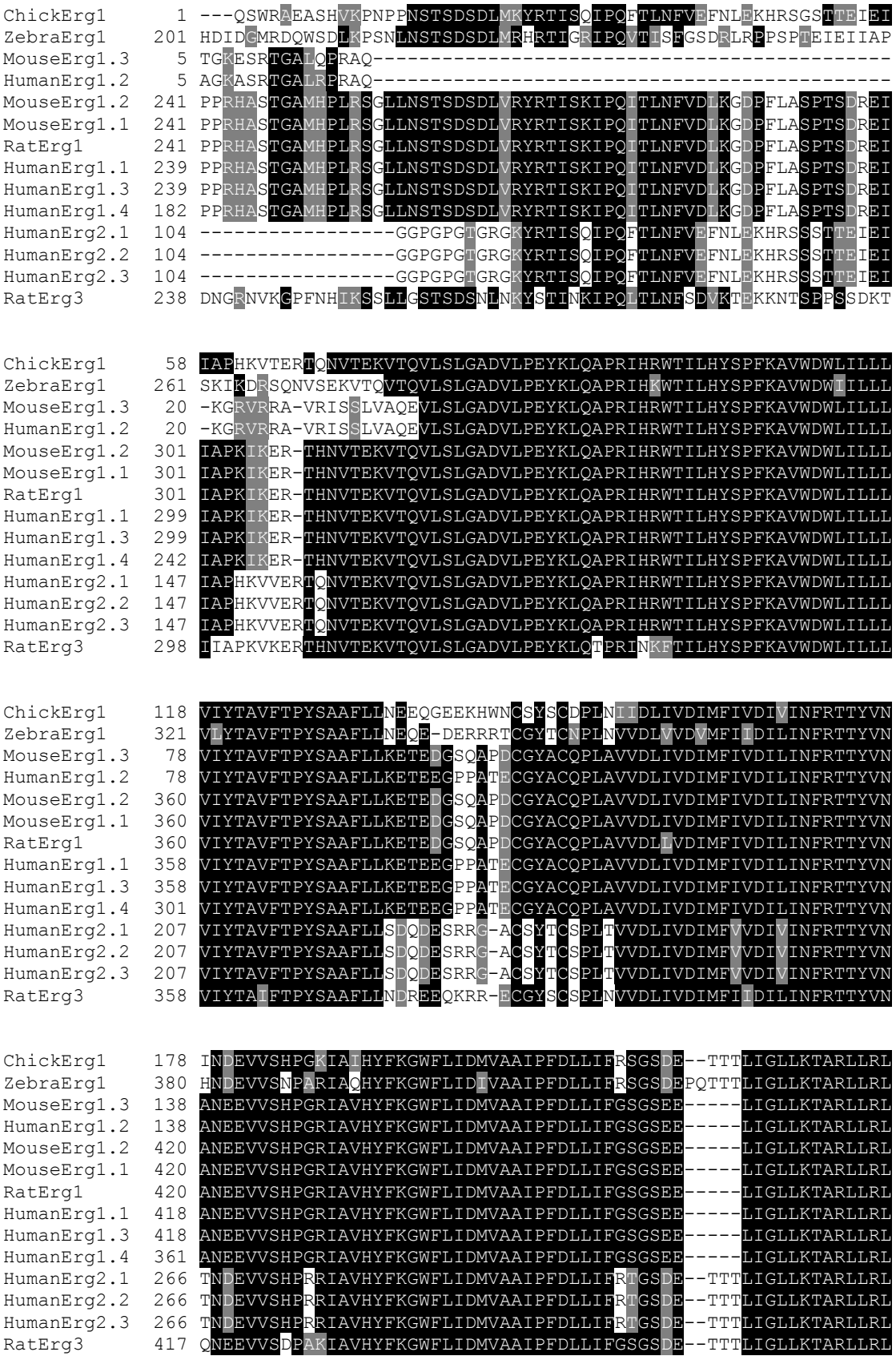
ChickErg1 1 ---QSWRAEASHVKPNPPNSTSDSDLMKYRTISQIPQFTLNFVEFNLEKHRSGSTTEIEI
ZebraErg1 201 HDIDGMRDQWSDLKPSNLNSTSDSDLMRHRTIGRIPQVTISFGSDRLRPPSPTEIEIIAP
MouseErg1.3 5 TGKESRTGALQPRAQ----------
HumanErg1.2 5 AGKASRTGALRPRAQ----------
MouseErg1.2 241 PPRHASTGAMHPLRSGLLNSTSDSDLVRYRTISKIPQITLNFVDLKGDPFLASPTSDREI
MouseErg1.1 241 PPRHASTGAMHPLRSGLLNSTSDSDLVRYRTISKIPQITLNFVDLKGDPFLASPTSDREI
RatErg1 241 PPRHASTGAMHPLRSGLLNSTSDSDLVRYRTISKIPQITLNFVDLKGDPFLASPTSDREI
HumanErg1.1 239 PPRHASTGAMHPLRSGLLNSTSDSDLVRYRTISKIPQITLNFVDLKGDPFLASPTSDREI
HumanErg1.3 239 PPRHASTGAMHPLRSGLLNSTSDSDLVRYRTISKIPQITLNFVDLKGDPFLASPTSDREI
HumanErg1.4 182 PPRHASTGAMHPLRSGLLNSTSDSDLVRYRTISKIPQITLNFVDLKGDPFLASPTSDREI
HumanErg2.1 104 ----------GGPGPGIGRGKYRTISQIPQFTLNFVEFNLEKHRSSSTTEIEI
HumanErg2.2 104 ----------GGPGPGIGRGKYRTISQIPQFTLNFVEFNLEKHRSSSTTEIEI
HumanErg2.3 104 ----------GGPGPGIGRGKYRTISQIPQFTLNFVEFNLEKHRSSSTTEIEI
RatErg3 238 DNGRNVKGPFNHIKSSLLGSTSDSNLNKYSTINKIPQLTLNFSDVKTEKKNTSPPSSDKT
ChickErg1 58 IAPHKVTERTQNVTEKVTQVLSLGADVLPEYKLQAPRIHRWTILHYSPFKAVWDWLILLL
ZebraErg1 261 SKIKDRSQNVSEKVTQVTQVLSLGADVLPEYKLQAPRIHKWTILHYSPFKAVWDWIILLL
MouseErg1.3 20 -KGRVRRA-VRISSLVAQEVLSLGADVLPEYKLQAPRIHRWTILHYSPFKAVWDWLILLL
HumanErg1.2 20 -KGRVRRA-VRISSLVAQEVLSLGADVLPEYKLQAPRIHRWTILHYSPFKAVWDWLILLL
MouseErg1.2 301 IAPKIKER-THNVTEKVTQVLSLGADVLPEYKLQAPRIHRWTILHYSPFKAVWDWLILLL
MouseErg1.1 301 IAPKIKER-THNVTEKVTQVLSLGADVLPEYKLQAPRIHRWTILHYSPFKAVWDWLILLL
RatErg1 301 IAPKIKER-THNVTEKVTQVLSLGADVLPEYKLQAPRIHRWTILHYSPFKAVWDWLILLL
HumanErg1.1 299 IAPKIKER-THNVTEKVTQVLSLGADVLPEYKLQAPRIHRWTILHYSPFKAVWDWLILLL
HumanErg1.3 299 IAPKIKER-THNVTEKVTQVLSLGADVLPEYKLQAPRIHRWTILHYSPFKAVWDWLILLL
HumanErg1.4 242 IAPKIKER-THNVTEKVTQVLSLGADVLPEYKLQAPRIHRWTILHYSPFKAVWDWLILLL
HumanErg2.1 147 IAPHKVVERTQNVTEKVTQVLSLGADVLPEYKLQAPRIHRWTILHYSPFKAVWDWLILLL
HumanErg2.2 147 IAPHKVVERTQNVTEKVTQVLSLGADVLPEYKLQAPRIHRWTILHYSPFKAVWDWLILLL
HumanErg2.3 147 IAPHKVVERTQNVTEKVTQVLSLGADVLPEYKLQAPRIHRWTILHYSPFKAVWDWLILLL
RatErg3 298 IIAPKVKERTHNVTEKVTQVLSLGADVLPEYKLQTPRINKFTILHYSPFKAVWDWLILLL
ChickErg1 118 VIYTAVFTPYSAAFLLNEEQGEEKHWNCSYSCDPLNIIDLIVDIMFIVDIVINFRTTYVN
ZebraErg1 321 VLYTAVFTPYSAAFLLNEQE-DERRRTCGYTCNPLNVVDLVVDVMFIIDILINFRTTYVN
MouseErg1.3 78 VIYTAVFTPYSAAFLLKETEDGSQAPDCGYACQPLAVVDLIVDIMFIVDILINFRTTYVN
HumanErg1.2 78 VIYTAVFTPYSAAFLLKETEEGPPATECGYACQPLAVVDLIVDIMFIVDILINFRTTYVN
MouseErg1.2 360 VIYTAVFTPYSAAFLLKETEDGSQAPDCGYACQPLAVVDLIVDIMFIVDILINFRTTYVN
MouseErg1.1 360 VIYTAVFTPYSAAFLLKETEDGSQAPDCGYACQPLAVVDLIVDIMFIVDILINFRTTYVN
RatErg1 360 VIYTAVFTPYSAAFLLKETEDGSQAPDCGYACQPLAVVDLLVDIMFIVDILINFRTTYVN
HumanErg1.1 358 VIYTAVFTPYSAAFLLKETEEGPPATECGYACQPLAVVDLIVDIMFIVDILINFRTTYVN
HumanErg1.3 358 VIYTAVFTPYSAAFLLKETEEGPPATECGYACQPLAVVDLIVDIMFIVDILINFRTTYVN
HumanErg1.4 301 VIYTAVFTPYSAAFLLKETEEGPPATECGYACQPLAVVDLIVDIMFIVDILINFRTTYVN
HumanErg2.1 207 VIYTAVFTPYSAAFLLSDQDESRRG-ACSYTCSPLTVVDLIVDIMFVVDIVINFRTTYVN
HumanErg2.2 207 VIYTAVFTPYSAAFLLSDQDESRRG-ACSYTCSPLTVVDLIVDIMFVVDIVINFRTTYVN
HumanErg2.3 207 VIYTAVFTPYSAAFLLSDQDESRRG-ACSYTCSPLTVVDLIVDIMFVVDIVINFRTTYVN
RatErg3 358 VIYTAIFTPYSAAFLLNDREEQKRR-ECGYSCSPLNVVDLIVDIMFITDILINFRTTYVN
ChickErg1 178 INDEVVSHPGKIAIHYFKGWFLIDMVAAIPFDLLIFRSGSDE--TTTLIGLLKTARLLRL
ZebraErg1 380 HNDEVVSNPARIAQHYFKGWFLIDIVAAIPFDLLIFRSGSDEPQTTTLIGLLKTARLLRL
MouseErg1.3 138 ANEEVVSHPGRIAVHYFKGWFLIDMVAAIPFDLLIFGSGSEE-----LIGLLKTARLLRL
HumanErg1.2 138 ANEEVVSHPGRIAVHYFKGWFLIDMVAAIPFDLLIFGSGSEE-----LIGLLKTARLLRL
MouseErg1.2 420 ANEEVVSHPGRIAVHYFKGWFLIDMVAAIPFDLLIFGSGSEE-----LIGLLKTARLLRL
MouseErg1.1 420 ANEEVVSHPGRIAVHYFKGWFLIDMVAAIPFDLLIFGSGSEE-----LIGLLKTARLLRL
RatErg1 420 ANEEVVSHPGRIAVHYFKGWFLIDMVAAIPFDLLIFGSGSEE-----LIGLLKTARLLRL
HumanErg1.1 418 ANEEVVSHPGRIAVHYFKGWFLIDMVAAIPFDLLIFGSGSEE-----LIGLLKTARLLRL
HumanErg1.3 418 ANEEVVSHPGRIAVHYFKGWFLIDMVAAIPFDLLIFGSGSEE-----LIGLLKTARLLRL
HumanErg1.4 361 ANEEVVSHPGRIAVHYFKGWFLIDMVAAIPFDLLIFGSGSEE-----LIGLLKTARLLRL
HumanErg2.1 266 TNDEVVSHPRRIAVHYFKGWFLIDMVAAIPFDLLIFRTGSDE--TTTLIGLLKTARLLRL
HumanErg2.2 266 TNDEVVSHPRRIAVHYFKGWFLIDMVAAIPFDLLIFRTGSDE--TTTLIGLLKTARLLRL
HumanErg2.3 266 TNDEVVSHPRRIAVHYFKGWFLIDMVAAIPFDLLIFRTGSDE--TTTLIGLLKTARLLRL
RatErg3 417 QNEEVVSDPAKIAVHYFKGWFLIDMVAAIPFDLLIFGSGSDE--TTTLIGLLKTARLLRL

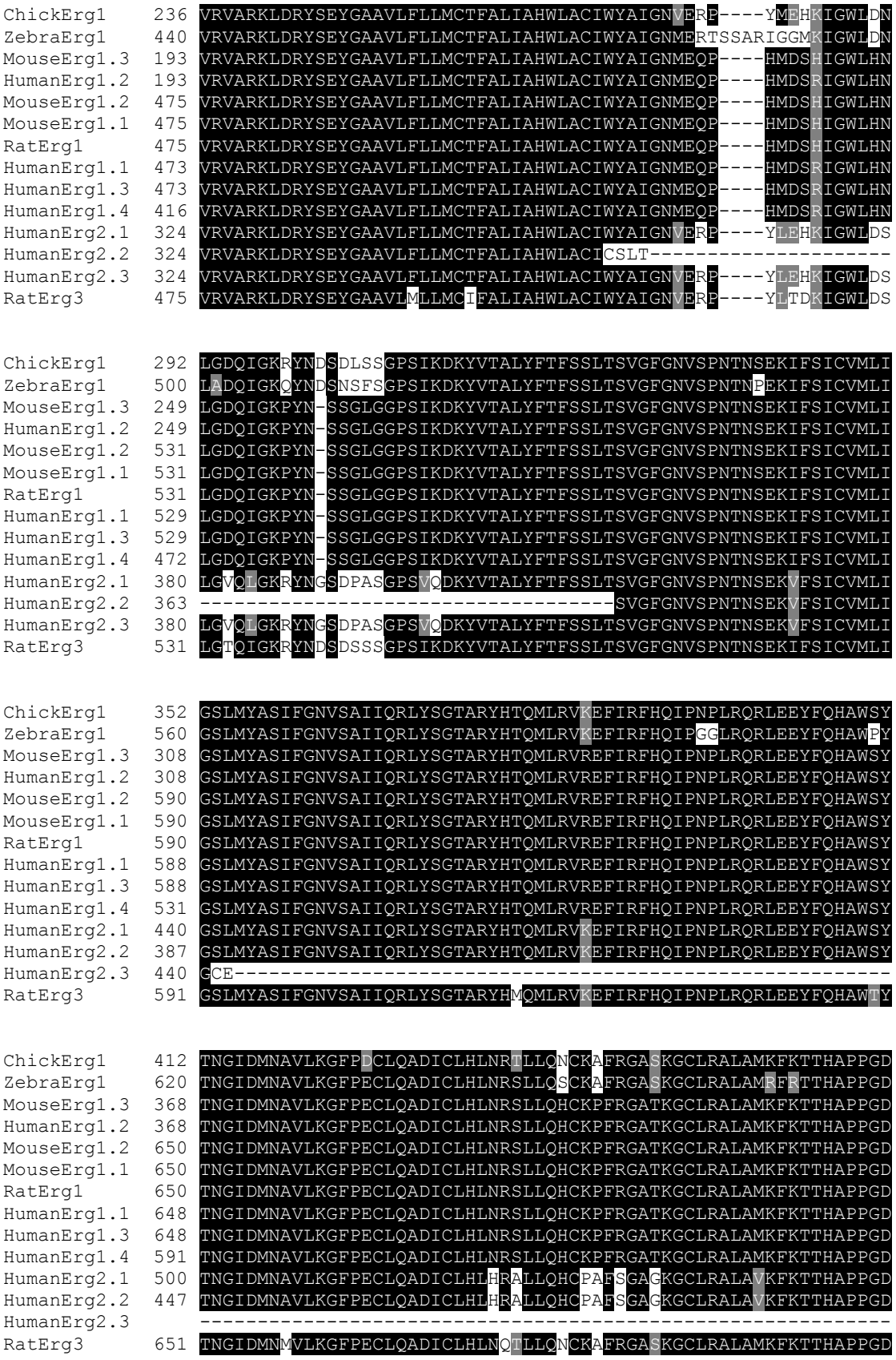
ChickErg1 236 VRVARKLDRYSEYGAAVLFLLMCTFALIAHWLACIWYAIGNVERP----YMEHKIGWLDN
ZebraErg1 440 VRVARKLDRYSEYGAAVLFLLMCTFALIAHWLACIWYAIGNMERTSSARIGGMKIGWLDN
MouseErg1.3 193 VRVARKLDRYSEYGAAVLFLLMCTFALIAHWLACIWYAIGNMEQP----HMDSHIGWLHN
HumanErg1.2 193 VRVARKLDRYSEYGAAVLFLLMCTFALIAHWLACIWYAIGNMEQP----HMDSRIGWLHN
MouseErg1.2 475 VRVARKLDRYSEYGAAVLFLLMCTFALIAHWLACIWYAIGNMEQP----HMDSHIGWLHN
MouseErg1.1 475 VRVARKLDRYSEYGAAVLFLLMCTFALIAHWLACIWYAIGNMEQP----HMDSHIGWLHN
RatErg1 475 VRVARKLDRYSEYGAAVLFLLMCTFALIAHWLACIWYAIGNMEQP----HMDSHIGWLHN
HumanErg1.1 473 VRVARKLDRYSEYGAAVLFLLMCTFALIAHWLACIWYAIGNMEQP----HMDSRIGWLHN
HumanErg1.3 473 VRVARKLDRYSEYGAAVLFLLMCTFALIAHWLACIWYAIGNMEQP----HMDSRIGWLHN
HumanErg1.4 416 VRVARKLDRYSEYGAAVLFLLMCTFALIAHWLACIWYAIGNMEQP----HMDSRIGWLHN
HumanErg2.1 324 VRVARKLDRYSEYGAAVLFLLMCTFALIAHWLACIWYAIGNVERP----YLEHKIGWLDS
HumanErg2.2 324 VRVARKLDRYSEYGAAVLFLLMCTFALIAHWLACICSLT----------
HumanErg2.3 324 VRVARKLDRYSEYGAAVLFLLMCTFALIAHWLACIWYAIGNVERP----YLEHKIGWLDS
RatErg3 475 VRVARKLDRYSEYGAAVLMLLMCIFALIAHWLACIWYAIGNVERP----YLTDKIGWLDS
ChickErg1 292 LGDQIGKRYNDSDLSSGPSIKDKYVTALYFTFSSLTSVGFGNVSPNTNSEKIFSICVMLI
ZebraErg1 500 LADQIGKQYNDSNSFSGPSIKDKYVTALYFTFSSLTSVGFGNVSPNTNPEKIFSICVMLI
MouseErg1.3 249 LGDQIGKPYN-SSGLGGPSIKDKYVTALYFTFSSLTSVGFGNVSPNTNSEKIFSICVMLI
HumanErg1.2 249 LGDQIGKPYN-SSGLGGPSIKDKYVTALYFTFSSLTSVGFGNVSPNTNSEKIFSICVMLI
MouseErg1.2 531 LGDQIGKPYN-SSGLGGPSIKDKYVTALYFTFSSLTSVGFGNVSPNTNSEKIFSICVMLI
MouseErg1.1 531 LGDQIGKPYN-SSGLGGPSIKDKYVTALYFTFSSLTSVGFGNVSPNTNSEKIFSICVMLI
RatErg1 531 LGDQIGKPYN-SSGLGGPSIKDKYVTALYFTFSSLTSVGFGNVSPNTNSEKIFSICVMLI
HumanErg1.1 529 LGDQIGKPYN-SSGLGGPSIKDKYVTALYFTFSSLTSVGFGNVSPNTNSEKIFSICVMLI
HumanErg1.3 529 LGDQIGKPYN-SSGLGGPSIKDKYVTALYFTFSSLTSVGFGNVSPNTNSEKIFSICVMLI
HumanErg1.4 472 LGDQIGKPYN-SSGLGGPSIKDKYVTALYFTFSSLTSVGFGNVSPNTNSEKIFSICVMLI
HumanErg2.1 380 LGVQLGKRYNGSDPASGPSVQDKYVTALYFTFSSLTSVGFGNVSPNTNSEKVFSICVMLI
HumanErg2.2 363 ----------SVGFGNVSPNTNSEKVFSICVMLI
HumanErg2.3 380 LGVQLGKRYNGSDPASGPSVQDKYVTALYFTFSSLTSVGFGNVSPNTNSEKVFSICVMLI
RatErg3 531 LGTQIGKRYNDSDSSSGPSIKDKYVTALYFTFSSLTSVGFGNVSPNTNSEKIFSICVMLI
ChickErg1 352 GSLMYASIFGNVSAIIQRLYSGTARYHTQMLRVKEFIRFHQIPNPLRQRLEEYFQHAWSY
ZebraErg1 560 GSLMYASIFGNVSAIIQRLYSGTARYHTQMLRVKEFIRFHQIPGGLRQRLEEYFQHAWPY
MouseErg1.3 308 GSLMYASIFGNVSAIIQRLYSGTARYHTQMLRVREFIRFHQIPNPLRQRLEEYFQHAWSY
HumanErg1.2 308 GSLMYASIFGNVSAIIQRLYSGTARYHTQMLRVREFIRFHQIPNPLRQRLEEYFQHAWSY
MouseErg1.2 590 GSLMYASIFGNVSAIIQRLYSGTARYHTQMLRVREFIRFHQIPNPLRQRLEEYFQHAWSY
MouseErg1.1 590 GSLMYASIFGNVSAIIQRLYSGTARYHTQMLRVREFIRFHQIPNPLRQRLEEYFQHAWSY
RatErg1 590 GSLMYASIFGNVSAIIQRLYSGTARYHTQMLRVREFIRFHQIPNPLRQRLEEYFQHAWSY
HumanErg1.1 588 GSLMYASIFGNVSAIIQRLYSGTARYHTQMLRVREFIRFHQIPNPLRQRLEEYFQHAWSY
HumanErg1.3 588 GSLMYASIFGNVSAIIQRLYSGTARYHTQMLRVREFIRFHQIPNPLRQRLEEYFQHAWSY
HumanErg1.4 531 GSLMYASIFGNVSAIIQRLYSGTARYHTQMLRVREFIRFHQIPNPLRQRLEEYFQHAWSY
HumanErg2.1 440 GSLMYASIFGNVSAIIQRLYSGTARYHTQMLRVKEFIRFHQIPNPLRQRLEEYFQHAWSY
HumanErg2.2 387 GSLMYASIFGNVSAIIQRLYSGTARYHTQMLRVKEFIRFHQIPNPLRQRLEEYFQHAWSY
HumanErg2.3 440 GCE----------
RatErg3 591 GSLMYASIFGNVSAIIQRLYSGTARYHMQMLRVKEFIRFHQIPNPLRQRLEEYFQHAWTY
ChickErg1 412 TNGIDMNAVLKGFPDCLQADICLHLNRTLLQNCKAFRGASKGCLRALAMKFKTTHAPPGD
ZebraErg1 620 TNGIDMNAVLKGFPECLQADICLHLNRSLLQSCKAFRGASKGCLRALAMRFRTTHAPPGD
MouseErg1.3 368 TNGIDMNAVLKGFPECLQADICLHLNRSLLQHCKPFRGATKGCLRALAMKFKTTHAPPGD
HumanErg1.2 368 TNGIDMNAVLKGFPECLQADICLHLNRSLLQHCKPFRGATKGCLRALAMKFKTTHAPPGD
MouseErg1.2 650 TNGIDMNAVLKGFPECLQADICLHLNRSLLQHCKPFRGATKGCLRALAMKFKTTHAPPGD
MouseErg1.1 650 TNGIDMNAVLKGFPECLQADICLHLNRSLLQHCKPFRGATKGCLRALAMKFKTTHAPPGD
RatErg1 650 TNGIDMNAVLKGFPECLQADICLHLNRSLLQHCKPFRGATKGCLRALAMKFKTTHAPPGD
HumanErg1.1 648 TNGIDMNAVLKGFPECLQADICLHLNRSLLQHCKPFRGATKGCLRALAMKFKTTHAPPGD
HumanErg1.3 648 TNGIDMNAVLKGFPECLQADICLHLNRSLLQHCKPFRGATKGCLRALAMKFKTTHAPPGD
HumanErg1.4 591 TNGIDMNAVLKGFPECLQADICLHLNRSLLQHCKPFRGATKGCLRALAMKFKTTHAPPGD
HumanErg2.1 500 TNGIDMNAVLKGFPECLQADICLHLHRALLQHCPAFSGAGKGCLRALAVKFKTTHAPPGD
HumanErg2.2 447 TNGIDMNAVLKGFPECLQADICLHLHRALLQHCPAFSGAGKGCLRALAVKFKTTHAPPGD
HumanErg2.3 ----------
RatErg3 651 TNGIDMNMVLKGFPECLQADICLHLNQTLLQNCKAFRGASKGCLRALAMKFKTTHAPPGD

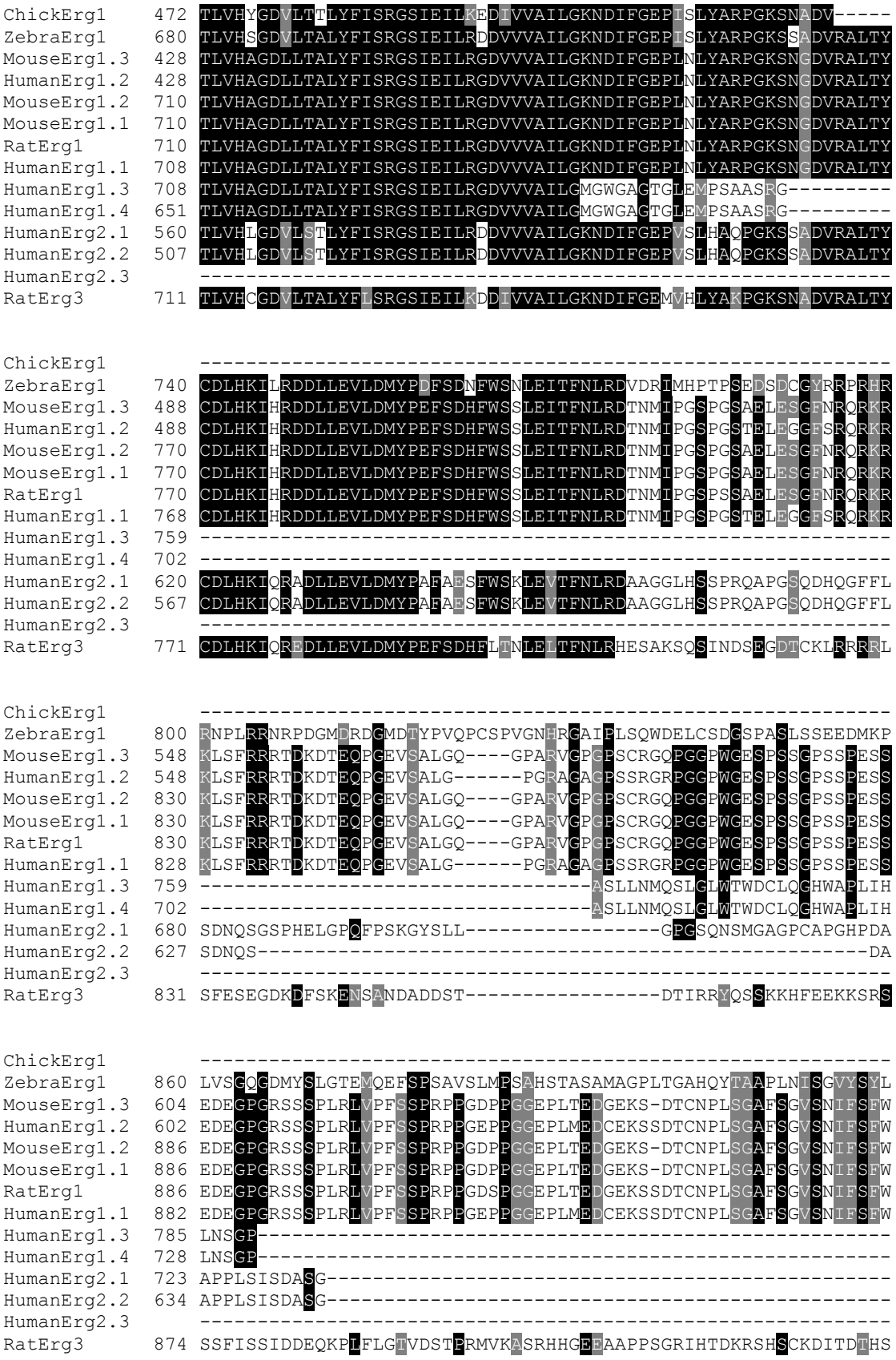
ChickErg1 472 TLVHYGDVLTTLYFISRGSIEILKEDIVVAILGKNDIFGEPISLYARPGKSNADV-----
ZebraErg1 680 TLVHSGDVLTALYFISRGSIEILRDDVVVAILGKNDIFGEPISLYARPGKSSADVRALTY
MouseErg1.3 428 TLVHAGDLLTALYFISRGSIEILRGDVVVAILGKNDIFGEPLNLYARPGKSNGDVRALTY
HumanErg1.2 428 TLVHAGDLLTALYFISRGSIEILRGDVVVAILGKNDIFGEPLNLYARPGKSNGDVRALTY
MouseErg1.2 710 TLVHAGDLLTALYFISRGSIEILRGDVVVAILGKNDIFGEPLNLYARPGKSNGDVRALTY
MouseErg1.1 710 TLVHAGDLLTALYFISRGSIEILRGDVVVAILGKNDIFGEPLNLYARPGKSNGDVRALTY
RatErg1 710 TLVHAGDLLTALYFISRGSIEILRGDVVVAILGKNDIFGEPLNLYARPGKSNGDVRALTY
HumanErg1.1 708 TLVHAGDLLTALYFISRGSIEILRGDVVVAILGKNDIFGEPLNLYARPGKSNGDVRALTY
HumanErg1.3 708 TLVHAGDLLTALYFISRGSIEILRGDVVVAILGMGWGAGTGLEMPSAASRG---------
HumanErg1.4 651 TLVHAGDLLTALYFISRGSIEILRGDVVVAILGMGWGAGTGLEMPSAASRG---------
HumanErg2.1 560 TLVHLGDVLSTLYFISRGSIEILRDDVVVAILGKNDIFGEPVSLHAQPGKSSADVRALTY
HumanErg2.2 507 TLVHLGDVLSTLYFISRGSIEILRDDVVVAILGKNDIFGEPVSLHAQPGKSSADVRALTY
HumanErg2.3 ----------
RatErg3 711 TLVHCGDVLTALYFLSRGSIEILKDDIVVAILGKNDIFGEMVHLYAKPGKSNADVRALTY
ChickErg1 ----------
ZebraErg1 740 CDLHKILRDDLLEVLDMYPDFSDNFWSNLEITFNLRDVDRIMHPTPSEDSDCGYRRPRHR
MouseErg1.3 488 CDLHKIHRDDLLEVLDMYPEFSDHFWSSLEITFNLRDTNMIPGSPGSAELESGFNRQRKR
HumanErg1.2 488 CDLHKIHRDDLLEVLDMYPEFSDHFWSSLEITFNLRDTNMIPGSPGSTELEGGFSRQRKR
MouseErg1.2 770 CDLHKIHRDDLLEVLDMYPEFSDHFWSSLEITFNLRDTNMIPGSPGSAELESGFNRQRKR
MouseErg1.1 770 CDLHKIHRDDLLEVLDMYPEFSDHFWSSLEITFNLRDTNMIPGSPGSAELESGFNRQRKR
RatErg1 770 CDLHKIHRDDLLEVLDMYPEFSDHFWSSLEITFNLRDTNMIPGSPSSAELESGFNRQRKR
HumanErg1.1 768 CDLHKIHRDDLLEVLDMYPEFSDHFWSSLEITFNLRDTNMIPGSPGSTELEGGFSRQRKR
HumanErg1.3 759 ----------
HumanErg1.4 702 ----------
HumanErg2.1 620 CDLHKIQRADLLEVLDMYPAFAESFWSKLEVTFNLRDAAGGLHSSPRQAPGSQDHQGFFL
HumanErg2.2 567 CDLHKIQRADLLEVLDMYPAFAESFWSKLEVTFNLRDAAGGLHSSPRQAPGSQDHQGFFL
HumanErg2.3 ----------
RatErg3 771 CDLHKIQREDLLEVLDMYPEFSDHFLTNLELTFNLRHESAKSQSINDSEGDTCKLRRRRL
ChickErg1 ----------
ZebraErg1 800 RNPLRRNRPDGMDRDGMDTYPVQPCSPVGNHRGAIPLSQWDELCSDGSPASLSSEEDMKP
MouseErg1.3 548 KLSFRRRTDKDTEQPGEVSALGQ----GPARVGPGPSCRGQPGGPWGESPSSGPSSPESS
HumanErg1.2 548 KLSFRRRTDKDTEQPGEVSALG------PGRAGAGPSSRGRPGGPWGESPSSGPSSPESS
MouseErg1.2 830 KLSFRRRTDKDTEQPGEVSALGQ----GPARVGPGPSCRGQPGGPWGESPSSGPSSPESS
MouseErg1.1 830 KLSFRRRTDKDTEQPGEVSALGQ----GPARVGPGPSCRGQPGGPWGESPSSGPSSPESS
RatErg1 830 KLSFRRRTDKDTEQPGEVSALGQ----GPARVGPGPSCRGQPGGPWGESPSSGPSSPESS
HumanErg1.1 828 KLSFRRRTDKDTEQPGEVSALG------PGRAGAGPSSRGRPGGPWGESPSSGPSSPESS
HumanErg1.3 759 ----------ASLLNMQSLGLWTWDCLQGHWAPLIH
HumanErg1.4 702 ----------ASLLNMQSLGLWTWDCLQGHWAPLIH
HumanErg2.1 680 SDNQSGSPHELGPQFPSKGYSLL----------GPGSQNSMGAGPCAPGHPDA
HumanErg2.2 627 SDNQS----------DA
HumanErg2.3 ----------
RatErg3 831 SFESEGDKDFSKENSANDADDST----------DTIRRMQSSKKHFEEKKSRS
ChickErg1 ----------
ZebraErg1 860 LVSGQGDMYSLGTEMQEFSPSAVSLMPSAHSTASAMAGPLTGAHQYTAAPLNISGVYSYL
MouseErg1.3 604 EDEGPGRSSSPLRLVPFSSPRPPGDPPGGEPLTEDGEKS-DTCNPLSGAFSGVSNIFSFW
HumanErg1.2 602 EDEGPGRSSSPLRLVPFSSPRPPGEPPGGEPLMEDCEKSSDTCNPLSGAFSGVSNIFSFW
MouseErg1.2 886 EDEGPGRSSSPLRLVPFSSPRPPGDPPGGEPLTEDGEKS-DTCNPLSGAFSGVSNIFSFW
MouseErg1.1 886 EDEGPGRSSSPLRLVPFSSPRPPGDPPGGEPLTEDGEKS-DTCNPLSGAFSGVSNIFSFW
RatErg1 886 EDEGPGRSSSPLRLVPFSSPRPPGDSPGGEPLTEDGEKSSDTCNPLSGAFSGVSNIFSFW
HumanErg1.1 882 EDEGPGRSSSPLRLVPFSSPRPPGEPPGGEPLMEDCEKSSDTCNPLSGAFSGVSNIFSFW
HumanErg1.3 785 LNSGP----------
HumanErg1.4 728 LNSGP----------
HumanErg2.1 723 APPLSISDASG----------
HumanErg2.2 634 APPLSISDASG----------
HumanErg2.3 ----------
RatErg3 874 SSFISSIDDEQKPTFLGTVDSTPRMVKASRHHGEEAAPPSGRIHTDKRSHSCKDITDTHS

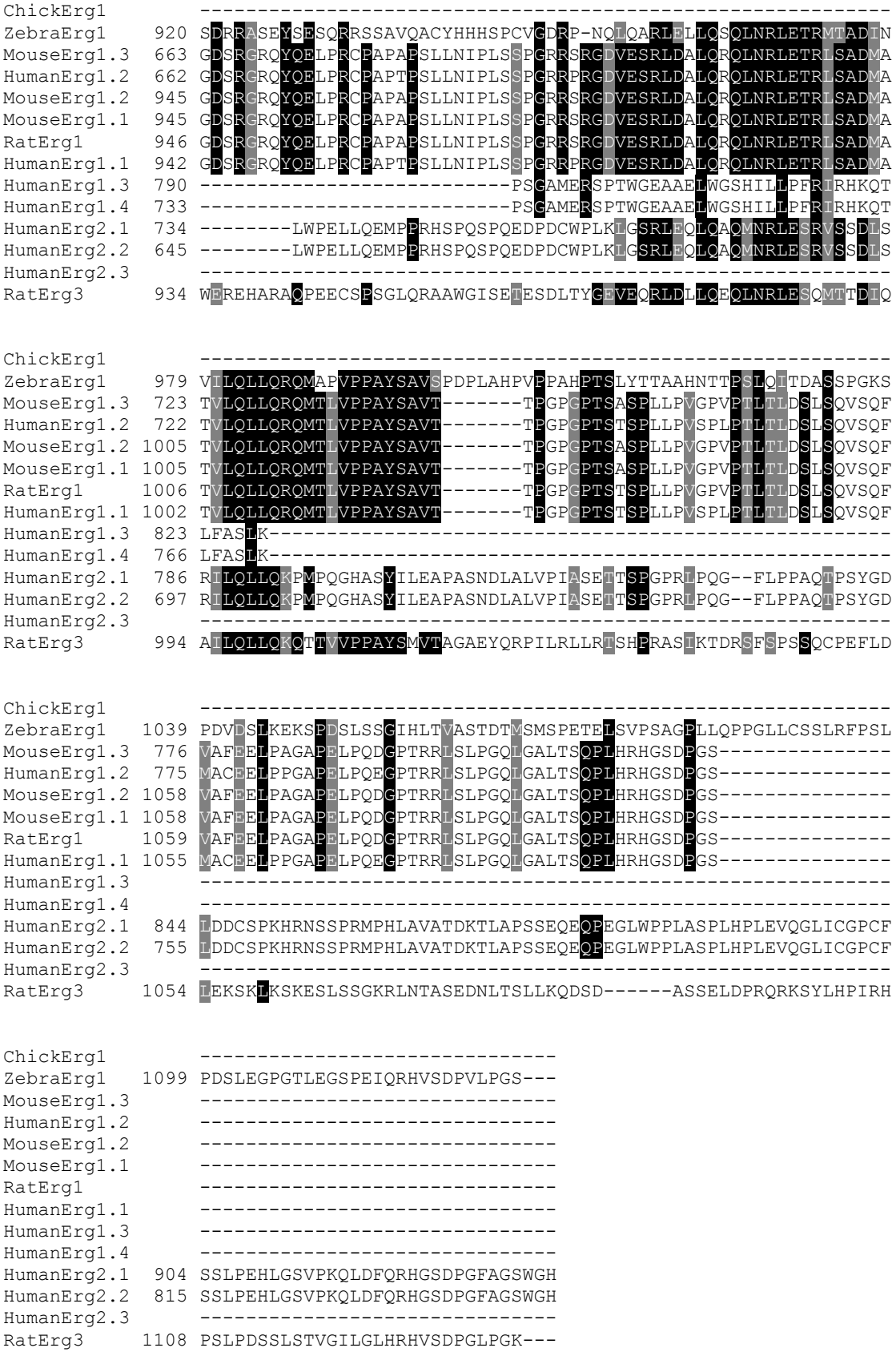
ChickErg1
ZebraErg1 920
MouseErg1.3 663
HumanErg1.2 662
MouseErg1.2 945
MouseErg1.1 945
RatErg1 946
HumanErg1.1 942
HumanErg1.3 790
HumanErg1.4 733
HumanErg2.1 734
HumanErg2.2 645
HumanErg2.3
RatErg3 934
ChickErg1
ZebraErg1 979
MouseErg1.3 723
HumanErg1.2 722
MouseErg1.2 1005
MouseErg1.1 1005
RatErg1 1006
HumanErg1.1 1002
HumanErg1.3 823
HumanErg1.4 766
HumanErg2.1 786
HumanErg2.2 697
HumanErg2.3
RatErg3 994
ChickErg1
ZebraErg1 1039
MouseErg1.3 776
HumanErg1.2 775
MouseErg1.2 1058
MouseErg1.1 1058
RatErg1 1059
HumanErg1.1 1055
HumanErg1.3
HumanErg1.4
HumanErg2.1 844
HumanErg2.2 755
HumanErg2.3
RatErg3 1054
ChickErg1
ZebraErg1 1099
MouseErg1.3
HumanErg1.2
MouseErg1.2
MouseErg1.1
RatErg1
HumanErg1.1
HumanErg1.3
HumanErg1.4
HumanErg2.1 904
HumanErg2.2 815
HumanErg2.3
RatErg3 1108

Appendix IV – *erg* cDNA cloned sequence

***Gallus gallus erg* (c*erg*) – 591 bp**

CAACATCATCGACCTCATCGTGGACATCATGTTCATCGTGGACATTGTCATCAACTTCCGCACCACCTACGTCAACATCAAC
GACGAGGTGGTGAGCCACCCGGGCAAGATTGCCATCCACTACTTCAAGGGCTGGTTCCTCATTGACATGGTGGCTGCCAT
CCCCTTTGATCTGCTCATCTTCCGCTCCGGCTCTGACGAGACCACCACCCTCATCGGTCTCCTGAAGACCGCCCGGCTGCTG
CGCCTGGTCCGTGTGGCCCGCAAGCTGGACCGCTACTCCGAGTACGGAGCAGCTGTGCTCTTCCTGCTCATGTGCACCTTT
GCCCTCATCGCCCACTGGCTGGCGTGCATCTGGTATGCCATTGGCAACGTGGAGCGGCCCTACATGGAGCATAAGATCGG
CTGGCTGGACAACCTGGGTGACCAGATCGGCAAGCGTTACAATGACAGCGACCTCTCCTCTGGGCCATCCATCAAGGATA
AATACGTCACTGCCCTCTACTTCACCTTCAGCAGCCTCACCAGCGTGGGCTTTGGCAACGTCTCGCCCAACACCAACTCTGA
GAAGATCTTCTCCATCTGCGTCATG

Appendix V – Hamburger and Hamilton Stages.